International Journal of Coal Geology 167 (2016) 48–64

Contents lists available at ScienceDirect

International Journal of Coal Geology

journal homepage: www.elsevier.com/locate/ijcoalgeo

Effect of lithostatic stress on methane sorption by coal: Theory vs. experiment and implications for predicting in-situ coalbed methane content

Jinfeng Liu [a,*], Christopher J. Spiers [a], Colin J. Peach [a], Sandrine Vidal-Gilbert [b]

[a] Department of Earth Sciences, Faculty of Geosciences, Utrecht University, 3584CD Utrecht, The Netherlands
[b] Total S.A., Unconventional Gas Resources, France

ARTICLE INFO

Article history:
Received 20 April 2016
Received in revised form 15 July 2016
Accepted 20 July 2016
Available online 27 July 2016

Keywords:
Sorption
Swelling
Coupled stress-strain-sorption equilibrium constant
Coal

ABSTRACT

Recent research has demonstrated that confining stresses applied to the solid framework of coal can reduce its gas sorption capacity by several percent to perhaps several tens of percent. To evaluate the magnitude of this effect more rigorously in relation to predicting in-situ coalbed methane (CBM) content, a better understanding of the effects of stress on methane sorption by coal is needed. In this paper, a previous thermodynamic model for the effects of stress on CO_2 sorption by coal is revised and applied to CH_4. The revised model predicts that in-situ CBM content is indeed determined not only by the geological factors generally considered, such as coal rank, coal composition, moisture content and temperature, but also by lithostatic or confining stress, which is usually ignored. This prediction is tested by means of experiments performed on a composite cylindrical sample of Brzeszcze 364 high volatile bituminous coal subjected to 10 MPa methane pressure at a temperature of 40°C, varying the hydrostatic stress or confining pressure in the range 11-43 MPa. In these experiments, we determined if CH_4 was desorbed as confining pressure was increased by subtracting the poroelastic expulsion of CH_4 from the total CH_4 expelled, assuming the former to equal the gas volume expelled in control experiments performed using Helium. The experimental results show that the equilibrium sorption capacity for CH_4 at 10 MPa gas pressure and 11 MPa confining pressure (1 MPa Terzaghi effective stress) was 0.808 mol/kg_{coal}. This was reduced by at least ~6% by increasing the confining pressure to 43 MPa (33 MPa effective stress), confirming the validity of our model. We apply our model to predict in-situ CBM concentration as a function of coal seam depth for dry, high volatile bituminous coal, assuming a geothermal gradient of 32°C/km. The results indicate a maximum CH_4 concentration of ~0.76 mol/kg_{coal} at a burial depth of ~900m, which is ~3% lower than conventional predictions. This reduction is minor but helps to explain why gas saturation is generally lower than expected from conventional sorption measurements on unconfined coal powders. More importantly, our results confirm that there is an intimate coupling between in-situ stress, strain and sorption in coal that needs to be considered in developing gas-enhanced CBM strategies.

1. Introduction

Subsurface coal seams typically consist of coal matrix (solid) material cut by a multiscale network of joints or cleats (Hol et al., 2012a; Laubach et al., 1998; Levine, 1996). These systems often contain large amounts of methane (CH_4) generated during the formation of the coal, i.e. during the so-called coalification process (Levine, 1993; Moore, 2012). Most of the methane ultimately trapped (~95% - 98%) is stored in the coal matrix via sorption (Gray, 1987; White et al., 2005). This can potentially be recovered economically in the form of natural gas, referred to as coalbed methane (CBM). The recovery or production of this methane is likewise termed CBM production (Levine, 1996; Moore, 2012). Compared to conventional natural gas reservoirs, such as sandstone formations, coal beds have low permeability, which usually limits primary CBM production by pressure depletion methods to 20-60% of the estimated reserves (White et al., 2005). Other gases, such as N_2, CO_2 and flue gas, have therefore been injected in attempts to enhance coalbed methane (ECBM) production (White et al., 2005). Of these, particular interest focuses on CO_2-ECBM, because coal preferentially adsorbs CO_2 over CH_4 (Fitzgerald et al., 2005; Gensterblum et al., 2014; Liu et al., 2015; Merkel et al., 2015; Ottiger et al., 2008; Pini et al., 2010), and can therefore be viewed as a potential lithology for combined ECBM plus geological storage of CO_2.

Besides coal reservoir permeability, CBM content is a key factor in assessing the economic feasibility of (E)CBM production. Estimation of CBM content is generally based on the sorption capacity of unstressed coal powders determined in the laboratory by means of manometric, volumetric or gravimetric measurements. These are performed under

* Corresponding author.
E-mail address: j.liu1@uu.nl (J. Liu).

http://dx.doi.org/10.1016/j.coal.2016.07.012

unconfined conditions, i.e. at zero conventional or Terzaghi effective stress where the fluid pressure equals the confining pressure and where sorption-induced swelling of the coal is opposed only by the fluid pressure (Busch and Gensterblum, 2011)

It is well-established that CH_4 sorption capacity is influenced by coal rank, coal composition, moisture content and temperature (Busch and Gensterblum, 2011; Bustin and Clarkson, 1998; Gensterblum et al., 2013, 2014; Moore, 2012). However, Pone et al. (2009) measured the CH_4 sorption capacity of bituminous coal (a cylinder of 25 mm in diameter) under both stressed (confined) and unstressed (unconfined) conditions using volumetric methods. They present evidence that confining stresses of 6.9 and 13.8 MPa caused a reduction in CH_4 sorption capacity of 85 and 91% respectively, at a CH_4 pressure of 3.8 MPa at room temperature. It is unclear, though, how much of this reduction was due to a) a direct effect of stress on equilibrium sorption capacity versus b) a reduction in the volume of coal sample that was accessible to CH_4 as sample permeability decreased with increasing confining stress. To obtain a reliable estimate of in-situ CBM content, a physically based and experimentally verified stress-strain-sorption model is required to describe the effect of in-situ stress on the CH_4 sorption capacity of coal at thermodynamic equilibrium.

Such a thermodynamic model was developed by Hol et al. (2012a) to describe how the equilibrium concentration of gas/fluid species adsorbed by coal is affected by compressive stresses applied in excess of the fluid pressure. This was experimentally proved to apply to CO_2 by the authors in the context of investigating CO_2-ECBM. However, a number of errors were made in deriving this model, which mean that though the form of the final equations obtained is correct, the physical meaning of the equilibrium constant for sorption that appears is not. Indeed, in the model by Hol et al., the equilibrium constant depends strongly on both temperature and gas pressure, whereas for a given reaction it should depend only on temperature (Chang, 2000; Hill, 2012). A corrected thermodynamic model is therefore needed to properly capture the physical process of gas adsorption by stressed coal, and to predict the true equilibrium CBM content of coal and the associated swelling strain response, under in-situ conditions where coal supports positive effective stress.

In the present paper, we revise the thermodynamic model developed by Hol et al. (2012a) for the effect of an applied stress state (σ_{ij}) on the concentration of gas/fluid species that can be adsorbed by coal, or by any other sorbent, and we show that the same result is obtained using both statistical mechanics and kinetic approaches. A corrected expression for thermodynamic equilibrium constant is thus obtained, which is confirmed to depend only on temperature for a given coal and gas species. To evaluate whether our model is applicable to adsorption of CH_4 by coal, and to the estimation of in-situ CBM content, we also report experiments. These were performed on a composite cylindrical sample of Brzeszcze high volatile bituminous coal to determine the dependence of adsorbed CH_4 concentration on applied effective stress. The experiments were conducted at a fixed temperature of 40°C and a fixed CH_4 pressure of 10 MPa, varying the applied hydrostatic pressure in the range 11-43 MPa (conventional effective stress of 1-33 MPa). The results show at least ~6% reduction in adsorbed CH_4 concentration at a confining pressure of 43 MPa (effective stress 33 MPa). We compare our model with our experimental results and show that our model successfully describes the adsorption process under stressed conditions. Finally, we discuss the implications for predicting in-situ CBM content.

2. Theoretical model

To gain clear insight into the effect of stress on sorption behavior, we begin by re-deriving the model presented by Hol et al. (2012a) for the sorption capacity of a single gas or fluid species under stressed conditions, using a corrected method. For simplicity, we henceforth use the term "gas", to cover both gas and (supercritical) fluid. We use the term "stressed coal" to refer to coal that supports a positive (conventional) effective stress in excess of the applied gas pressure. Compressive stresses and gas pressure are measured positive, as is swelling strain.

In our derivation, we consider the closed system specified in Fig. 1, consisting of a small coal matrix cube of mass m and side l (≤1mm), surrounded by a pure gas phase (α) present at constant pressure P, absolute temperature T and chemical potential μ_g. We assume the gas phase to be pressurized via a movable outer boundary subjected to a constant pressure boundary condition. The coal matrix cube, also at uniform temperature T, is independently subjected to a general stress state σ_{ij} via a permeable loading frame that allows free access of gas to the coal (Fig. 1). Following Hol et al. (2011, 2012a), the cube is considered homogeneous in structure and composition at the particle length scale l, but may be anisotropic in properties. It is further assumed to contain nano-pores only, so that there is no Darcian flow and negligible storage of free (unadsorbed) gas. In other words, the coal particle is so small that it is cleat free and can take up gas only by molecular diffusion and adsorption. The coal particle is accordingly elastic but not poro-elastic. Lastly, we assume that the coal cube hosts n_s localized adsorption sites, each of which consists of a potential well capable of trapping a single molecule of the gas α, as illustrated in Fig. 2.

2.1. Attachment energy for adsorption of a single molecule by stressed coal

2.1.1. Energy / Entropy balance for the solid phase

When a single molecule of gas species α is reversibly adsorbed by the coal matrix cube (Fig. 1), the first and second laws of thermodynamics for the solid phase (subscript s) yield the Gibbs equation

$$\Delta U_s^{\sigma} = -\sigma_{ij}\Delta\varepsilon_{ij}^{ads} l^3 + T\Delta S_s^{\sigma} + \mu_s^{\sigma} \tag{1}$$

In this relation, ΔU_s^{σ} (J•molecule^{-1}) is the change in internal energy of the solid phase. The term $-\sigma_{ij}\Delta\varepsilon_{ij}^{ads} l^3$ represents the stress-strain work done on the surroundings as the coal swells against the total applied stress σ_{ij} by an adsorption-induced swelling strain $\Delta\varepsilon_{ij}^{ads}$, ΔS_s^{σ} (J•K^{-1}•molecule^{-1}) is the entropy change of the solid, and μ_s^{σ} (J•molecule^{-1}) is the chemical potential of the adsorbed molecule within the potential well associated with the sorption site that traps it (see Fig. 2). Note that we treat the adsorbed gas molecules as being a "dissolved" component of the solid phase here, as opposed to assuming an independently identifiable adsorbed phase (following the treatment of Myers (2002) for stress-free sorption).

If the volume change of the coal particle associated with the swelling strain $\Delta\varepsilon_{ij}^{ads}$ per adsorbed molecule is Ω_0 (the partial molecular volume of the adsorbed gas in m^3•molecule^{-1}), then the particle undergoes a volumetric strain $\Delta\varepsilon_v^{ads} = {}^{\Omega_0}/_{l^3} = \Delta\varepsilon_{11}^{ads} + \Delta\varepsilon_{22}^{ads} + \Delta\varepsilon_{33}^{ads}$ per molecule adsorbed. This can be viewed as associated with an isotropic swelling strain, or mean extensional strain, of $\Delta\bar{\varepsilon}^{ads} = {}^{\Delta\varepsilon_v^{ads}}/_3 = {}^{\Omega_0}/_{3l^3}$. We can hence split $\Delta\varepsilon_{ij}^{ads}$ into an isotropic swelling strain component $\Delta\bar{\varepsilon}^{ads}\delta_{ij} = ({}^{\Omega_0}/_{3l^3})\delta_{ij}$ and a deviatoric component $\Delta\varepsilon_{ij}'^{ads} = \Delta\varepsilon_{ij}^{ads} - ({}^{\Omega_0}/_{3l^3})\delta_{ij}$, where δ_{ij} is the Kronecker delta (Fig. 3). The deviatoric strain components can further be specified as $\Delta\varepsilon_{ij}'^{ads} = \Delta\bar{\varepsilon}^{ads}A_{ij} = ({}^{\Omega_0}/_{3l^3})A_{ij}$, where $A_{ij} = {}^{\Delta\varepsilon_{ij}'^{ads}}/_{\Delta\bar{\varepsilon}^{ads}}$ is a second rank tensor expressing the anisotropy of sorption-induced swelling strain. Hence, we can write $\Delta\varepsilon_{ij}^{ads} = \Delta\bar{\varepsilon}^{ads}\delta_{ij} + \Delta\varepsilon_{ij}'^{ads} = (\delta_{ij} + A_{ij})({}^{\Omega_0}/_{3l^3})$. Similarly expressing σ_{ij} in terms of the means stress ($\bar{\sigma} = {}^{\sigma_{kk}}/_3$) and deviatoric stress ($\sigma_{ij}' = \sigma_{ij} - \bar{\sigma}\delta_{ij}$) components, now means that the stress-strain work term in Eq. (1) can be written as $(\bar{\sigma} + {}^1/_3\sigma_{ij}'A_{ij})\Omega_0$ (Hol et al., 2012a).

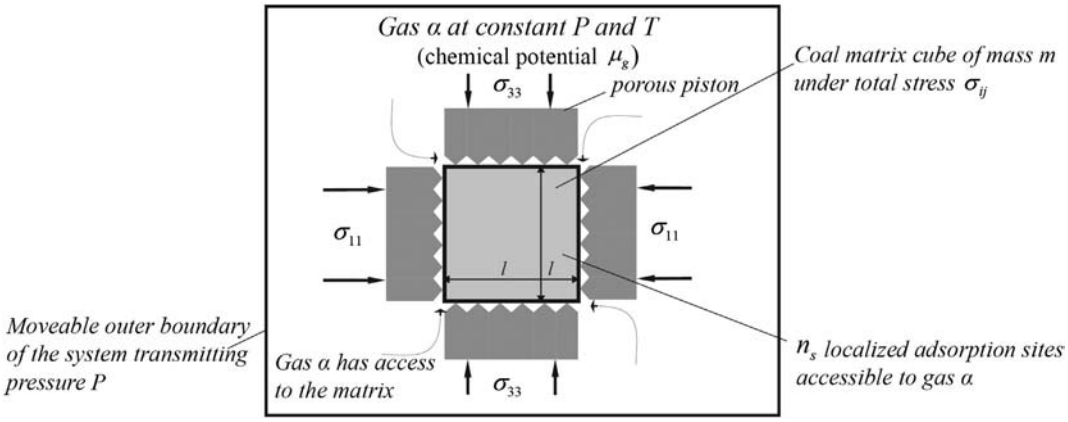

Fig. 1. Representative volume of coal matrix material used in the present analysis of adsorption under conditions of constant stress σ_{ij}. The representative volume consists of a small cube of coal matrix material, of mass m and side l ($l \leq 1$ mm), containing n_s localized adsorption sites accessible to gas α. The cube is so small that it is free of cleats and consists entirely of nanoporous coal matrix material. Once the coal particle is exposed to gas α at constant pressure P and at constant temperature T, it is accordingly assumed to take up gas α only by diffusion and adsorption.

The internal energy change for the solid phase in Eq. (1) accordingly becomes,

$$\Delta U_s^\sigma = -\left(\overline{\sigma} + {}^1/_3\sigma'_{ij}A_{ij}\right)\Omega_0 + T\Delta S_s^\sigma + \mu_s^\sigma \tag{2a}$$

$$\text{so that} \quad \mu_s^\sigma = \Delta U_s^\sigma - T\Delta S_s^\sigma + \left(\overline{\sigma} + {}^1/_3\sigma'_{ij}A_{ij}\right)\Omega_0 = \Delta F_s^\sigma + \left(\overline{\sigma} + {}^1/_3\sigma'_{ij}A_{ij}\right)\Omega_0 \tag{2b}$$

where ΔF_s^σ (J•molecule^{-1}) represents the change in Helmholtz free energy of the coal matrix particle for adsorption of a single molecule. Note that both Ω_0 and ΔF_s^σ are assumed here to be insensitive to the stress state supported by the coal particle, and to the gas pressure.

When the coal matrix cube is subjected only to the reference pressure P_0, defined as the gas pressure for which the activity $a_g = 1$, then $\sigma_{ij} = P_0\delta_{ij}$, $\overline{\sigma} = P_0$, $\sigma_{ij}' = 0$ and Eq. (2b) modifies to

$$\mu_s^{P_0} = \Delta F_s^{P_0} + P_0\Omega_0 \tag{3}$$

where $\mu_s^{P_0}$ (see Fig. 2) is the potential of the molecule in the adsorbed state at temperature T and reference gas pressure P_0. In addition, $\mu_s^{P_0}$ can be expressed as $\mu_s^{P_0} = \mu_s^0 + \Delta\mu^*(T, P_0)$, where μ_s^0 is the potential in vacuo at absolute zero, i.e. the minimum energy at ground state (c.f. Hill, 2012), and $\Delta\mu^*(T, P_0)$ is the energy of the adsorbed molecule at temperature
T and reference pressure P_0 measured with respect to the ground state. Since P_0 is a constant for a given gas, this means the potential $\mu_s^{P_0}$ depends only on temperature T.

When the coal matrix cube is subjected to a general gas pressure P under otherwise stress-free conditions, we now get $\sigma_{ij} = P\delta_{ij}$ and Eq. (2b) yields

$$\mu_s^P = \Delta F_s^P + P\Omega_0 \tag{4}$$

where μ_s^P (see Fig. 2) is the potential of the adsorbed molecule at temperature T and gas pressure P, and clearly depends on both.

Assuming $\Delta F_s^{P_0} \approx \Delta F_s^P \approx \Delta F_s^\sigma$ as already mentioned, and using Eqs. (2b), (3) and (4), we hence obtain the relations

$$\mu_s^P = \mu_s^{P_0} + (P - P_0)\Omega_0 \tag{5a}$$

$$\mu_s^\sigma = \mu_s^{P_0} + \left(\overline{\sigma} - P_0 + {}^1/_3\sigma'_{ij}A_{ij}\right)\Omega_0 \tag{5b}$$

$$\mu_s^\sigma = \mu_s^P + \left(\overline{\sigma} - P + {}^1/_3\sigma'_{ij}A_{ij}\right)\Omega_0 \tag{5c}$$

between the potentials $\mu_s^{P_0}$, μ_s^P and μ_s^σ represented in Fig. 2,

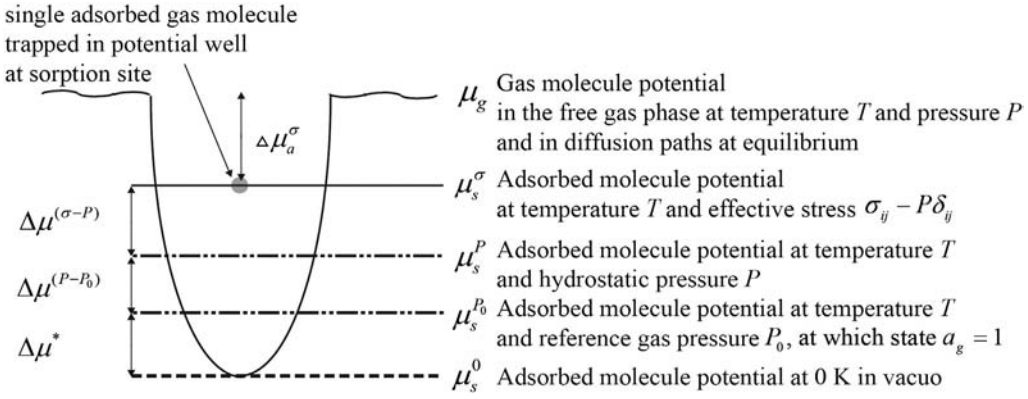

Fig. 2. Potential well associated with an adsorption site present in coal matrix material under stress σ_{ij} (see Fig. 1). Here μ_g represents the chemical potential of a single molecule present in free gas phase at pressure P and temperature T, and present in the diffusion paths inside the matrix at equilibrium. The quantity $\mu_s^\sigma(\sigma, T)$ represents the potential of a single adsorbed gas molecule located in the potential well under stress state $\sigma_{ij} > P\delta_{ij}$. This consists of the potential μ_s^P of the adsorbed gas molecule under unconfined hydrostatic (effective stress-free) conditions, where $\sigma_{ij} = P\delta_{ij}$, plus the extra potential $\Delta\mu^{(\sigma-P)}$ related to the applied effective stress $\sigma_{ij} - P\delta_{ij}$. The quantity $\mu_s^P(P, T)$ itself consists of the potential $\mu_s^{P_0}(T)$, measured at temperature T and reference gas pressure P_0 at which $a_g = 1$, plus the potential $\Delta\mu^{(P-P_0)}$ related to the excess gas pressure P-P_0. The quantity $\mu_s^{P_0}(T)$ is only temperature dependent for a given gas at reference pressure P_0, consisting of the potential μ_s^0 at absolute 0 in vacuo, plus the potential $\Delta\mu^*(T, P_0)$. Finally, $\Delta\mu_a^\sigma$ represents the total change in potential associated with adsorbing a single molecule from the gas phase into the solid, yielding $\Delta\mu_a^\sigma = \mu_s^{P_0}(T) + \Delta\mu^{(P-P_0)} + \Delta\mu^{(\sigma-P)} - \mu_g$. Here δ_{ij} is Kronecker delta.

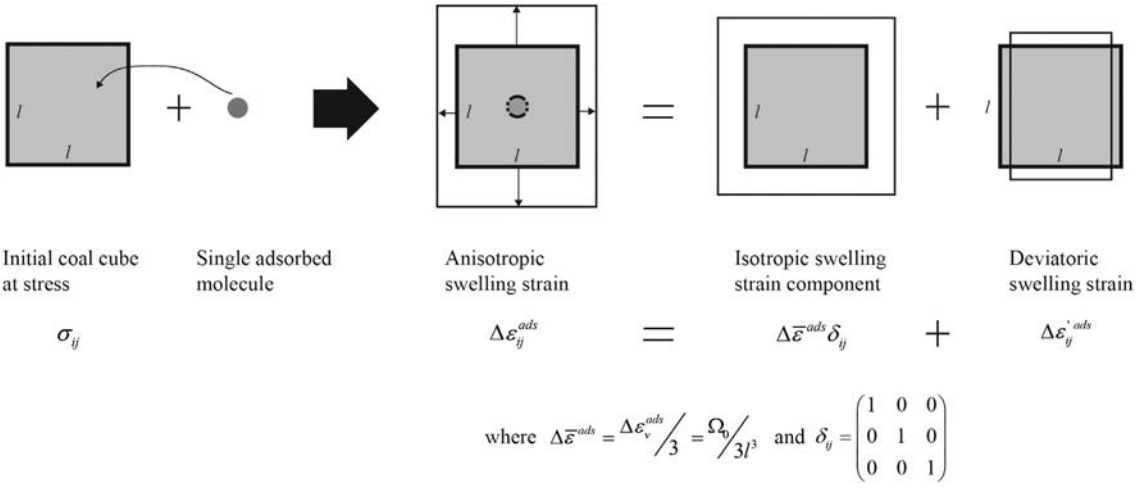

Fig. 3. Illustration of anisotropic swelling strain due to adsorption of a single gas molecule by coal cube of edge dimension l and volume l^3. $\Delta\varepsilon_v^{ads} = \Delta\varepsilon_{kk}^{ads}$ is the volumetric strain produced by adsorbing a single molecule having partial molecular volume Ω_0.

2.1.2. Energy / Entropy balance for the gas phase

For the gas phase (subscript g) in Fig. 1, the internal energy change that occurs when a single molecule is removed by adsorption is given, via the Gibbs equation analogous to Eq. (1), as

$$\Delta U_g^P = P\Omega_g^P + T\Delta S_g^P - \mu_g \tag{6a}$$

$$\text{so that } \mu_g = -\left(\Delta U_g^P - T\Delta S_g^P\right) + P\Omega_g^P = -\Delta F_g^P + P\Omega_g^P \tag{6b}$$

In this case, Ω_g^P (m^3•$molecule^{-1}$) is the molecular volume of the gas phase at pressure P and temperature T, ΔS_g (J•K^{-1}• $molecule^{-1}$) is the entropy change associated with removing one molecule from the gas, and ΔF_g^P (J• $molecule^{-1}$) is the corresponding change in Helmholtz energy of the gas phase. The quantity μ_g represents the chemical potential of a single gas molecule (Fig. 2), which can be expressed from the thermodynamics of fluid systems as

$$\mu_g = \mu_{g0} + kT\ln a_g \tag{7}$$

where $a_g = a_g(P,T)$ is the chemical activity of the free gas at pressure P and temperature T, and where μ_{g0} is the potential of gas species α at the reference pressure P_0, for which $a_g = 1$. Of course, when the gas pressure $P = P_0$, Eq. (6b) becomes

$$\mu_{g0} = -\Delta F_g^{P_0} + P_0\Omega_g^{P_0} \tag{8}$$

where $\Omega_g^{P_0}$ is the molecular volume of gas phase at pressure P_0 and temperature T.

2.1.3. Combined solid-gas system

For the combined solid-gas system (subscript a), with the solid at stress σ_{ij}, the gas at pressure P and the system at uniform temperature T, we now get, adding (2a) and (6a),

$$\Delta\mu_a^\sigma = \mu_s^\sigma - \mu_g = \Delta U_a^\sigma + P\left(\Omega_0 - \Omega_g^P\right) - T\Delta S_a^\sigma + (\bar{\sigma} - P)\Omega_0 + {}^1/_3\sigma_{ij}'A_{ij}\Omega_0 \tag{9a}$$

$$\text{or } \Delta\mu_a^\sigma = \mu_s^\sigma - \mu_g = \Delta F_a^\sigma + P\left(\Omega_0 - \Omega_g^P\right) + (\bar{\sigma} - P)\Omega_0 + {}^1/_3\sigma_{ij}'A_{ij}\Omega_0 \tag{9b}$$

Here, ΔU_a^σ (J•$molecule^{-1}$) is the internal energy change of the system, ΔS_a^σ (J•K^{-1}• $molecule^{-1}$) is its entropy change, ΔF_a^σ (J• $molecule^{-1}$) is the corresponding change in Helmholtz free energy, and $\Delta\mu_a{}^\sigma$ (J• $molecule^{-1}$) is the change in potential associated with the adsorbed molecule, i.e. the change in the free energy of the system due to the attachment of the adsorbed molecule. Physically, the attachment energy $\Delta\mu_a^\sigma$ represents (negative) energy change (i.e. the energy released from the system) when a single gas molecule is adsorbed by the stressed coal at gas pressure P and system temperature T, or conversely, the energy that must be supplied to remove a single adsorbed molecule localized in the potential well into the free phase at these conditions.

Similarly, from (3) minus (8), the change in potential of the combined solid-gas system due to adsorption of a single molecule by unstressed coal at the reference gas pressure P_0 and temperature T, , is

$$\Delta\mu_a^{P_0} = \mu_s^{P_0} - \mu_{g0} = \Delta F_a^{P_0} + P_0\left(\Omega_0 - \Omega_g^{P_0}\right) \tag{10}$$

This attachment energy $\Delta\mu_a^{P_0}$ depends only on temperature for a given coal type and gas species. Likewise, when the coal matrix cube is subjected to gas pressure P only, i.e. to hydrostatic conditions defined $\sigma_{ij} = P\delta_{ij}$, the attachment energy, from Eqs. (4) minus (6b), is given

$$\Delta\mu_a^P = \mu_s^P - \mu_g = \Delta F_a^P + P\left(\Omega_0 - \Omega_g^P\right) \tag{11}$$

where the quantity $\Delta\mu_a^P$ is now a function of temperature and pressure.

2.2. Adsorption energy for n molecules

For a total population of adsorption sites n_s, we assume that each adsorption site remains empty or else takes up one gas molecule. We further assume that there is no interaction between adsorbed molecules. Then from combination theory, the number of different ways that n adsorbed molecules can be distributed over the n_s available sites can be written as $W^i = \frac{n_s!}{n!(n_s-n)!}$. Following numerous previous authors (e.g. Hill, 2012; Hol et al., 2012a; Tuin and Stein, 1995), this contributes a configurational entropy term $\Delta S^i = -k\ln W^i$, and hence an energy term $-kT\ln W^i$ to the potential of the adsorbed molecules and hence to the overall change in energy that occurs when n molecules of species α are adsorbed. The change in energy of the solid due to adsorption of n molecules is accordingly given not as $n\mu_s^\sigma$ but as

$$\Delta\Phi_s = n\mu_s^\sigma - kT\ln\frac{n_s!}{n!(n_s-n)!} \tag{12}$$

while the total energy change of the coal-gas system due to adsorption

of n molecules is given as

$$\Delta\Phi_a = n\Delta\mu_a^{\sigma} - kT\ln\frac{n_s!}{n!(n_s-n)!} \tag{13}$$

where k is Boltzmann's constant.

By comparison with the Gibbs free energy for a reaction under hydrostatic conditions, written in generic form as $(\Delta G)_{P,T} = \Delta U - T\Delta S + P\Delta V$, it is evident from Eqs. (2b), (9a), (12) and (13) that the quantities $\mu_s^{\sigma}(\sigma_{ij},T)$, $\Delta\mu_a(\sigma_{ij},P,T)$, $\Delta\Phi_s(\sigma_{ij},T,n)$ and $\Delta\Phi_a(\sigma_{ij},P,T,n)$ are all Gibbs-like free energies generalized to stressed conditions, i.e. to include stress-strain work independently of $P\Delta V$ work. Now, the present Langmuir-type adsorption process can be formulated as the reaction

$$\alpha_{(gas)} + C^*_{(solid)} \rightleftharpoons \alpha : C^*_{(solid)}$$

where α represents molecules in the free gas phase, C^* represents sorption sites in the stressed coal matrix, and $\alpha:C^*$ represents the complex formed when a gas molecule is bound to an adsorption site (Butt et al., 2006; Hol et al., 2012a). The total free energy change for adsorption of n molecules via this reaction is of course

$$\Delta\Phi_R = \Delta\Phi_{\alpha:C^*} - \Delta\Phi_{C^*} - n\mu_g \tag{14}$$

where $\Delta\Phi_{\alpha:C^*}$ is the free energy contributed to the solid phase by n filled sorption sites and $\Delta\Phi_{C^*}$ is the free energy contributed to the solid by n sites before sorption. The term $(\Delta\Phi_{\alpha:C^*} - \Delta\Phi_{C^*})$ represents the change in free energy of the coal matrix due to adsorption of n molecules, so it must be equal to $\Delta\Phi_s$. Inserting this into Eq. (14) gives

$$\Delta\Phi_R = \Delta\Phi_s - n\mu_g \tag{15}$$

At the same time, subtracting Eqs. (12) from (13) gives $\Delta\Phi_a - \Delta\Phi_s = n(\Delta\mu_a^{\sigma} - \mu_s^{\sigma})$, which on inserting $\Delta\mu_a^{\sigma} = \mu_s^{\sigma} - \mu_g$ from Eqs. (9a) and (9b) yields

$$\Delta\Phi_a = \Delta\Phi_s - n\mu_g \tag{16}$$

Eqs. (15) and (16) accordingly demonstrate that the total energy change $\Delta\Phi_a$ of a stressed coal plus gas system due to adsorption of n molecules is identical to the free energy change $\Delta\Phi_R$ for the Langmuir-type reaction.

2.3. Chemical potential per molecule for n molecules adsorbed by stressed coal

Focusing now on the solid system only, if n molecules are adsorbed, the sorption of a further dn molecules leads to an internal energy change given by the infinitesimal equivalent of the Gibbs equation presented in Eq. (1), written here as $dU_s = -\sigma_{ij}d\varepsilon_{ij}^{ads} + TdS_s + \mu_s dn$ or $\mu_s dn = dU_s - TdS_s + \sigma_{ij}d\varepsilon_{ij}^{ads}$, where μ_s is the molecule-specific potential of the n adsorbed molecules. Again by analogy with the generic Gibbs energy change $(\Delta G)_{P,T} = \Delta U - T\Delta S + P\Delta V$ in hydrostatic systems, the term $\mu_s dn$ can be identified as the free energy change $(d\Phi_s)_{\sigma_{ij},T} = dU_s - TdS_s + \sigma_{ij}d\varepsilon_{ij}^{ads} = \mu_s dn$ associated with adsorption by a non-hydrostatically stressed solid. It follows that $\mu_s = \left(\frac{\partial\Phi_s}{\partial n}\right)_{\sigma_{ij},T}$, where $\Phi_s = \Phi_{s0} + \Delta\Phi_s$ is the total free energy of the stressed solid plus n adsorbed gas molecules, Φ_{s0} is the free energy of the stressed solid when $n = 0$, and $\Delta\Phi_s$ is the change in energy due to adsorption of n molecules as given by Eq. (12). Since Φ_{s0} is a constant at constant σ_{ij} and T, it further follows that

$$\mu_s = \left(\frac{\partial\Delta\Phi_s}{\partial n}\right)_{\sigma_{ij},T} \tag{17}$$

Applying Stirling's approximation $\ln x! \approx x(\ln x - 1)$ for large x to Eq. (12), and differentiating the expression for $\Delta\Phi_s$ obtained, now leads to the result

$$\mu_s = \mu_s^{\sigma} + kT\ln\left(\frac{\theta}{1-\theta}\right) \tag{18}$$

where $\theta = n/n_s$ is the concentration of adsorbed gas measured in terms of adsorption site occupancy.

2.4. Equilibrium concentration of adsorbed species α in stressed coal

2.4.1. Site occupancy at equilibrium and equilibrium constant

We now assume that the adsorption proceeds until equilibrium is reached. At that point, the chemical potential of the adsorbed molecules (μ_s) must be equal to that of the gas molecules (μ_g), so that

$$\mu_s \equiv \mu_s^{\sigma} + kT\ln\left(\frac{\theta}{1-\theta}\right) = \mu_g \tag{19}$$

Using Eqs. (5a), (5b), (5c) and (7) for μ_s^{σ} and μ_g, we hence obtain the following expressions for the equilibrium concentration of adsorbed molecules per available site n_s, namely

$$\theta = \frac{a_g\exp\left(\frac{\mu_{g0}-\mu_s^{P_0}}{kT}\right)\exp\left(\frac{-(\overline{\sigma}-P_0)\Omega_0}{kT}\right)\exp\left(\frac{-\sigma'_{ij}A_{ij}\Omega_0}{3kT}\right)}{1 + a_g\exp\left(\frac{\mu_{g0}-\mu_s^{P_0}}{kT}\right)\exp\left(\frac{-(\overline{\sigma}-P_0)\Omega_0}{kT}\right)\exp\left(\frac{-\sigma'_{ij}A_{ij}\Omega_0}{3kT}\right)} \tag{20a}$$

$$\text{or}\quad \theta = \frac{a_g\exp\left(\frac{\mu_{g0}-\mu_s^{P}}{kT}\right)\exp\left(\frac{-(\overline{\sigma}-P)\Omega_0}{kT}\right)\exp\left(\frac{-\sigma'_{ij}A_{ij}\Omega_0}{3kT}\right)}{1 + a_g\exp\left(\frac{\mu_{g0}-\mu_s^{P}}{kT}\right)\exp\left(\frac{-(\overline{\sigma}-P)\Omega_0}{kT}\right)\exp\left(\frac{-\sigma'_{ij}A_{ij}\Omega_0}{3kT}\right)} \tag{20b}$$

Taking the conventional definition of a thermodynamic equilibrium constant as being temperature dependent only (see Chang, 2000; Hill, 2012), the true thermodynamic equilibrium constant for sorption in our model (Eqs. (20a) and (20b)) is the quantity given

$$K^0 = \exp\left(\frac{\mu_{g0}-\mu_s^{P_0}}{kT}\right) \tag{21}$$

Here, the term $(\mu_s^{P_0} - \mu_{g0}) = \Delta\mu_a^{P_0}$ (Eq. (10)) represents the potential change of the coal-gas system due to adsorption of a single gas molecule in the hydrostatic reference state at which $P = P_0$, $a_g = 1$ and $\sigma_{ij} = P_0\delta_{ij}$. In line with conventional definitions, this is 'the standard free energy change' for the sorption reaction (Hill, 2012). By contrast, the term

$$K = \exp\left(\frac{\mu_{g0}-\mu_s^{P}}{kT}\right) \tag{22}$$

is not a true equilibrium constant, as it is clearly seen, from Eqs. (4) and (5a), that μ_s^P and hence K depend on gas pressure P via the partial molecular volume Ω_0, such that

$$K = K^0\exp\left(\frac{-(P-P_0)\Omega_0}{kT}\right) \tag{23}$$

An alternative way to obtain Eqs. (20a) to (23), describing equilibrium between the stressed solid and the surrounding gas, is to minimise the free energy Φ_a of the combined solid-gas system. If the free energy of the system before adsorption is Φ_{a0}, then $\Phi_a = \Phi_{a0} + \Delta\Phi_a$, when $\Delta\Phi_a$ is the total free energy change due to sorption of n molecules, given by Eq. (13). Since Φ_{a0} is a constant at fixed σ_{ij}, P and T, $\left(\frac{\partial\Phi_a}{\partial n}\right)_{\sigma_{ij},P,T} = \left(\frac{\partial\Delta\Phi_a}{\partial n}\right)_{\sigma_{ij},P,T}$. At equilibrium, Φ_a is minimum and its derivative must equal zero. Differentiating Eq. (13) for $\Delta\Phi_a$ with respect

to n, after applying Stirling's approximation, and setting $\left(\frac{\partial \Delta\Phi_a}{\partial n}\right)_{\sigma_{ij},P,T} = 0$, yields

$$\mu_a^{\sigma} + kT \ln\left(\frac{\theta}{1-\theta}\right) = 0 \tag{24}$$

Since $\Delta\mu_a^{\sigma} = \mu_s^{\sigma} - \mu_g$ (Eqs. (9a) and (9b)), and since the molecule specific potential $\mu_s \equiv \mu_s^{\sigma} + kT \ln\left(\frac{\theta}{1-\theta}\right)$ (Eq. (18)), we hence obtain $\mu_s \equiv \mu_s^{\sigma} + kT \ln\left(\frac{\theta}{1-\theta}\right) = \mu_g$, which is identical to the equilibrium condition expressed in Eq. (19), and thus yields the same expression for θ as given in Eqs. (20a) and (20b).

The essential difference between our result for equilibrium adsorbed concentration θ given in Eqs. (20a) and (20b) (specifically in 20b) and that obtained by Hol et al. (2011, 2012a) lies in the quantity K given in Eq. (22). Using our notation, Hol et al. obtained $K = \exp\left(\frac{\mu_{g0} + \mu_g - \mu_s^P}{kT}\right)$. The main error made by Hol et al. (2011, 2012a) in their derivation is that, by incorrectly writing $\Phi_a = \Phi_{a0} + \Delta\Phi_a$ (see above) as $\Phi_a = \Phi_{a0} + \Delta\Phi_a - n\mu_g$, they set $\mu_s = \left(\frac{\partial \Delta\Phi_a}{\partial n}\right)_{\sigma_{ij},P,T}$ instead of $\mu_s = \left(\frac{\partial \Delta\Phi_s}{\partial n}\right)_{\sigma_{ij},T}$ as in our Eqs. (17) and (18). Their equilibrium condition is accordingly incorrect and the result they obtain, though similar to Eqs. (20a) and (20b) in form, contains $(\mu_{g0} + \mu_g)$ instead of μ_{g0}.

2.4.2. Equilibrium concentration of adsorbed species α in mol/kg

The total number of localized adsorption sites (in mol) present in one kilogram of coal matrix, C_s (mol/kg) for a specific gas species, is now assumed to be a characteristic of the (macro)molecular structure of the solid. It therefore depends only on coal type, specifically through the reference potential $\mu_s^{P_0} = \mu_s^0 + \Delta\mu^*$ (see Fig. 2), and hence through equilibrium constant K^0. C_s is further assumed to be independent of the adsorbed concentration, gas pressure, state of stress and temperature. Using Eqs. (20a)-(22), and switching to molar quantities, we thus obtain the following final expressions for adsorbed concentration of species α in mol/kg, namely

$$C = C_s\theta = \frac{C_s a_g K^0 \exp\left(\frac{-(\overline{\sigma} - P_0)V_0}{RT}\right)\exp\left(\frac{-\sigma_{ij}' A_{ij} V_0}{3RT}\right)}{1 + a_g K^0 \exp\left(\frac{-(\overline{\sigma} - P_0)V_0}{RT}\right)\exp\left(\frac{-\sigma_{ij}' A_{ij} V_0}{3RT}\right)} \tag{25a}$$

$$\text{or } C = C_s\theta = \frac{C_s a_g K \exp\left(\frac{-(\overline{\sigma} - P)V_0}{RT}\right)\exp\left(\frac{-\sigma_{ij}' A_{ij} V_0}{3RT}\right)}{1 + a_g K \exp\left(\frac{-(\overline{\sigma} - P)V_0}{RT}\right)\exp\left(\frac{-\sigma_{ij}' A_{ij} V_0}{3RT}\right)} \tag{25b}$$

where $V_0 = N_A\Omega_0$ is partial molar volume of the adsorbed gas species, N_A is the Avogadro constant, and R is the gas constant. At low gas pressures (low a_g) and/or when the solid supports high stresses (high $\overline{\sigma}$ or σ_{ij}'), site occupancies are low with $\theta << 1$, and the right hand term in the denominator of Eqs. (20a), (20b), (25a) and (25b) becomes $<<1$. Eqs. (20a), (20b) hence (25a), (25b) can therefore be simplified to yield

$$C \approx C_s a_g K^0 \exp\left(\frac{-(\overline{\sigma} - P_0)V_0}{RT}\right)\exp\left(\frac{-\sigma_{ij}' A_{ij} V_0}{3RT}\right) \tag{26a}$$

$$\text{or } C \approx C_s a_g K \exp\left(\frac{-(\overline{\sigma} - P)V_0}{RT}\right)\exp\left(\frac{-\sigma_{ij}' A_{ij} V_0}{3RT}\right) \tag{26b}$$

The present, revised models (20, 25) and their simplified forms for low gas pressure (e.g. 26) demonstrate that the sorption process is controlled by the combined effects of five factors: 1) the activity $a_g(P,T)$ and/or the chemical potential of the free gas phase, 2) the reference potential $\mu_s^{P_0}(T)$ or $(\mu_{g0} - \mu_s^{P_0})$ and hence the equilibrium constant K^0, which depend on temperature only, 3) the adsorption site concentration per kilogram of coal C_s, 4) the partial molar volume V_0 of the adsorbed gas species, which depends on coal rank and gas species, and 5) the total stress state σ_{ij} supported by the coal matrix. We note that the present analysis applies to "monolayer adsorption", i.e. one-site/one-molecule adsorption, of any sorbate by any stress-supporting solid phase. It accordingly should apply to "monolayer adsorption" of CO_2, CH_4, and N_2 by coal. Importantly, our results (25, 26) are identical to those obtained by other possible approaches, specifically statistical mechanics and kinetic approaches. To demonstrate this equivalence, these approaches are presented in Appendix A.

2.5. Adsorption under stress-free conditions

If the solid (coal) phase is exposed to gas at pressure P under otherwise stress-free conditions, i.e. with $\sigma_{ij} = P\delta_{ij}$, our adsorption model (Eqs. (25a) and (25b)) reduces to

$$C = C_s\theta = \frac{C_s a_g K^0 \exp\left(\frac{-(P - P_0)V_0}{RT}\right)}{1 + a_g K^0 \exp\left(\frac{-(P - P_0)V_0}{RT}\right)} \tag{27a}$$

$$\text{or } C = C_s\theta = \frac{C_s a_g K}{1 + a_g K} \tag{27b}$$

If the free gas outside the solid behaves as an ideal gas, then a_g can be replaced by P. Moreover, if the gas pressure P is close to the reference pressure $P_0 = 0.1$ MPa = 1bar, then $K = K^0 \exp\left(\frac{-(P - P_0)\Omega_0}{kT}\right)$ (Eq. (23)) approaches K^0 and becomes insensitive to gas pressure. Under these conditions, Eq. (27b) reduces to the well-known Langmuir isotherm $C = \frac{C_L K_L P}{1 + K_L P}$, where C_L and K_L are the Langmuir constants (Langmuir, 1918) and are identified as C_s and K in Eq. (27b) respectively. K_L is accordingly seen to depend on gas pressure P via Ω_0. Note, however, that in the classical Langmuir model, swelling of the adsorbent is neglected so that $\Omega_0 = 0$, forcing the Langmuir constant K_L to appear pressure independent with $K_L = K = K^0$ (Myers and Monson, 2002).

On the basis of the adsorption model for unstressed conditions expressed in Eq. (27b), Liu et al. (2015) developed thermodynamic models for swelling of unconfined coal matrix due to adsorption of mixed gases. The "equilibrium constant" defined in those models is not the true equilibrium constant K^0 expressed in Eq. (21), but the quantity K expressed in Eq. (22), which is a function of temperature and gas pressure. However, the validity of the model equations presented by Liu et al. (2015) is unaffected by this as is the physical basis put forward by Liu et al. for the selective sorption of mixed gases by coal. The parameters obtained by Liu et al., in fitting their mixed gas model to experimental data for mixed gases at different partial pressures, might be slightly affected, however, as are all fits for K or K_L obtained by fitting the classical Langmuir equation to gas sorption data.

2.6. Adsorption under hydrostatic applied stress

The present relations for θ and C (i.e. Eqs. (20a), (20b), (25a), (25b), (26a) and (26b)) apply for a general three-dimensional stress σ_{ij} applied to coal matrix material. For the special case of a hydrostatic (i.e. isotropic) stress state $\sigma > P$, the mean stress $\overline{\sigma} = \sigma$ and the deviatoric components of the stress tensor disappear, so that $\sigma_{ij}' = 0$. In this case, our expression for adsorbed concentration (Eqs. (25a) and

(25b)) reduces to

$$C = C_s\theta = \frac{C_s a_g K^0 \exp\left(\frac{-(\sigma - P_0)V_0}{RT}\right)}{1 + a_g K^0 \exp\left(\frac{-(\sigma - P_0)V_0}{RT}\right)} \quad (28a)$$

$$\text{or } C = C_s\theta = \frac{C_s a_g K \exp\left(\frac{-(\sigma - P)V_0}{RT}\right)}{1 + a_g K \exp\left(\frac{-(\sigma - P)V_0}{RT}\right)} \quad (28b)$$

Note that this result for an applied isotropic stress σ applies regardless of whether swelling properties of coal are isotropic or anisotropic (i.e. independently of A_{ij}). Interestingly, the same results also apply for isotropic coal subjected to an anisotropic stress, because then $\mathbf{A_{ij} = 0}$ in Eqs. (25a) and (25b). An expression of the same form as Eq. (28b) was obtained by Hol et al. (2011, 2012a) for sorption by coal subjected to a hydrostatic stress $\sigma > P$. Once again, however, the quantity K was erroneously given as $K = \exp(\frac{\mu_{g0} + \mu_g - \mu_s^P}{kT})$ and not as $K = \exp(\frac{\mu_{g0} - \mu_s^P}{kT})$.

2.7. Adsorption under stressed versus unstressed conditions: A comparison

The adsorbed concentration C at equilibrium under an applied stress state $\sigma_{ij} > P\delta_{ij}$ or $\sigma > P$, expressed through Eqs. (25b) and (28b), is clearly lower than that under stress-free conditions, where $\sigma_{ij} = P\delta_{ij}$, predicted by 27b or by the classical Langmuir relation. This is due to the stress-strain work done that must be done in association with sorption-induced swelling against the positive Terzaghi effective stress $(\overline{\sigma} - P)$ and against the deviatoric stress σ'_{ij} under stressed conditions. Under in-situ conditions in a coal seam, the lithostatic stress state means that in general both $\sigma_{ij} > P\delta_{ij}$ and $\overline{\sigma} > P$.

On this basis, our model for adsorption under a hydrostatic effective stress $(\sigma - P)$, i.e. Eq. (28b), predicts a reduction in sorption capacity relative to the hydrostatic state where $\sigma = P$ (Eq. (27b)) given by $\frac{C^\sigma}{C^P} = \frac{\exp(\frac{-(\sigma-P)V_0}{RT})(1+a_g K)}{1+a_g K \exp(\frac{-(\sigma-P)V_0}{RT})}$. Similar reductions are predicted for more general stress states. To calculate the magnitude of the resulting reduction in adsorption capacity, the partial molecular volume Ω_0 or partial molar volume V_0 of the adsorbed gas species must be known. Assuming V_0 is insensitive to stress state, this can be derived from sorption induced swelling experiments on either stressed or unstressed coal, via the expression $e_v^{ads} = C\rho V_0$ (Hol et al., 2012a; Hol and Spiers, 2012). Here e_v^{ads} represents the engineering volumetric swelling strain caused by sorption, C represents the adsorbed concentration (mol/kg$_{coal}$) and ρ represents the density of coal (kg/m^3). For CO_2, V_0 typically lies in the range $1 - 2 \times 10^{-5}$ m^3/mol (Hol et al., 2011, 2012a; Hol and Spiers, 2012), and its value for CH_4 is similar to that for CO_2 (Day et al., 2010).

3. Experimental test of the effect of hydrostatic stress on adsorption of CH_4 by coal

As shown above, our models (i.e. Eqs. (25b) and (28b)) predict that in situ stress reduces the CH_4 sorption capacity of coal compared with the predictions made by the widely used Langmuir model which neglects sorption-induced swelling and hence the effect of stress. The present experiments were conducted to test our model for applied hydrostatic stresses $\sigma > P$, i.e. to test Eq. (28b) explicitly. The previous experimental study performed by Pone et al. (2009) suggests that the application of a positive Terzaghi effective stress to solid cylindrical coal samples (25 mm in diameter) indeed leads to a reduction in CH_4 sorption capacity. However, it is unclear in the study of Pone et al. how much of this reduction was due to a) a direct effect of stress on equilibrium sorption capacity, versus b) a reduction in the volume of the coal sample that was accessible to CH_4 through a decrease in sample permeability with increasing confining stress. To more rigorously test our thermodynamic model, the present experiments were performed on a single composite coal sample containing artificially introduced transport paths, which minimized the influence of the positive Terzaghi effective stress on sample permeability and accessibility of the sample volume to CH_4.

3.1. Methods

To achieve our aim, we applied the volumetric method (Busch and Gensterblum, 2011; Hol et al., 2012a) to measure the CH_4 expulsion from a solid coal sample exposed to a constant CH_4 pressure of 10 MPa at a temperature of 40°C, increasing the applied hydrostatic confining pressure in steps from 11 MPa to 43 MPa, and allowing the sample to reach equilibrium. Note that the expulsion of CH_4 measured here is due to a) free methane expulsion from the pore volume/cleats of the sample caused by poro-elastic effects, and b) any desorption from the matrix. To obtain the true amount of desorption of CH_4 from the coal matrix, we applied the same experimental procedures used for CH_4 expulsion measurement to perform expulsion experiments using He (non-sorbing gas). In this way, we could correct our measured data for gas expulsion from the sample due to poro-elastic effects.

3.1.1. Sample preparation and treatment

The sample material used in present experiments consisted of high volatile bituminous coal collected from Brzeszcze 364, Poland. The composition and properties of the coal are described by Hol et al. (2011). Specifically, the Brezeszcze coal used in this study contains 2.9% moisture content, and 5.2% ash content.

In order to a) speed up CH_4 equilibration with the sample, while minimizing the free CH_4 volume in the sample, and b) ensure the amount of CH_4 desorbed from the solid sample could be measured accurately enough, we prepared a composite cylindrical sample of the Brzeszcze coal consisting of a stack of 20 coal discs, as shown in Fig. 4a. Each disc consisted of a flat-ground coal matrix disc, of 25 mm in diameter and 2.2 to 3.3 mm in thickness, cored normal to bedding. In contrast to the composite sample prepared by Hol et al. (2012a), who employed a single 1 mm hole drilled through the center of each disc in similar experiments using CO_2, we drilled 5 cylindrical holes of 1 mm in diameter through each disc, as shown in Fig. 4b. This was done to further shorten the effective diffusion path into the discs and to reduce equilibration time, which for CH_4 is longer than for CO_2 at given PT conditions (Busch and Gensterblum, 2011; Pone et al., 2009). To further shorten CH_4 diffusion paths in the coal matrix, we pre-treated the sample with CH_4 at 10 MPa pressure, to generate micro-fractures in the matrix (Hol et al., 2012b).

The mass and bulk volume of the composite sample, measured before the CH_4 expulsion experiment, were 34.69 g and 28.59 ml, respectively. To seal the sample from the confining medium used to apply a hydrostatic stress, the sample was enclosed in a 1mm thick, annealed lead (Pb) jacket, by welding brass end-cups into the lead jacket, as shown in Fig. 4c. Using lead allowed us to accurately measure the volumetric deformation of the sample due to CH_4 injection, and to avoid jacket failure when the confining pressure reached the higher values used. Before assembling the sample inside the apparatus and drying it there in-situ, we pre-dried the sample in a high vacuum oven at an in-situ temperature of 40°C for more than a week (in fact ~12 days) to remove the residual water, air and gas.

3.1.2. Apparatus

The apparatus used in the present experiments (Fig. 5) consisted of a stainless steel pressure vessel (30 mm inner diameter), housing the jacketed sample, placed in a temperature controlled water bath. The jacked sample was hydrostatically pressurized externally, within the

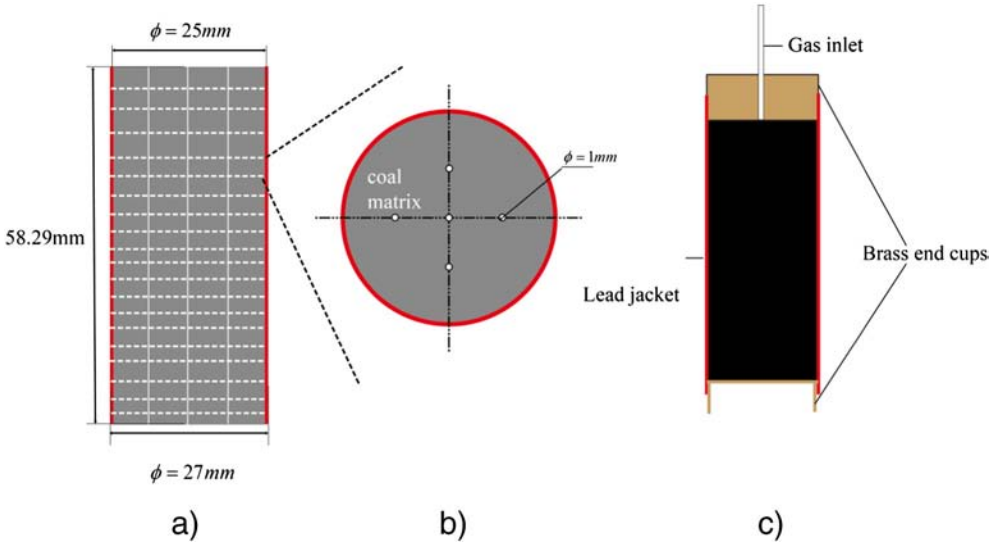

Fig. 4. Schematic illustration of composite coal sample. (a) Cylindrical stack of 20, flat-ground coal matrix discs of 25 mm in diameter and 2.2-3.3 mm in thickness. (b) The positioning of the 5 cylindrical holes of 1mm in diameter drilled in each disc. c) The composite sample sealed in 1 mm thick Pb jacket.

vessel, using water as a confining fluid, driven by an ISCO 65D servo-controlled volumetric pump. He or CH_4 were introduced into the sample via a high pressure CH_4/He line passing through the closure nut of the pressure vessel. The internal CH_4/He pressure was controlled by an independent ISCO 65D volumetric (syringe) pump (c.f. Hol and Spiers, 2012). Both ISCO pumps were operated in constant pressure mode in the present experiments, allowing the internal and external pressures to be controlled to within ±0.049 MPa. The volume change measured by these pumps was taken as a measure of the bulk volumetric strain of the sample (H_2O pump), and the volume of CH_4/He injected into or expelled from the sample (CH_4/He pump). To control sample temperature, the vessel was placed into the Lauda water bath at 40 ± 0.1°C. A foam-polystyrene box was also constructed around the syringe pumps and water bath to control the air temperature around the setup at 38.6 ± 0.2°C, using an internal lamp, fan and CAL 9900 PID-controller (c.f. Hol and Spiers, 2012). Temperature was measured at the locations shown in Fig. 5 (T_{pt}) using PT-100 sensors with a resolution of 0.01°C.

3.1.3. Data acquisition

The temperature of the system was recorded using a National Instruments, 16-channel DAOPad-6015 A/D convertor and VI-logger data acquisition system, at a sampling rate of 0.2 Hz. The pump pressure and volume signals were directly obtained in 16 bit digital form from the ISCO 65D Pumps, at a sampling rate of 0.2 Hz using ISCO 65D Panel software.

3.1.4. Leakage rate calibration

Both the gas and water systems were tested for leaks before the experiments, at experimental conditions and with no sample present. The tests took ~1 day (versus ~30 days for the CH_4 runs). The pumps were operated in constant pressure mode and changes in both gas and water volume were recorded versus time. The CH_4/He volume decreased linearly (R^2>0.98) with time when maintaining a constant gas pressure of 10 MPa. The corresponding data yielded a leakage rate for CH_4 of ~12.3 μl/h and for He of ~52.6 μl/h. No measureable leakage could be detected using the H_2O pump at a pressure of 11 MPa.

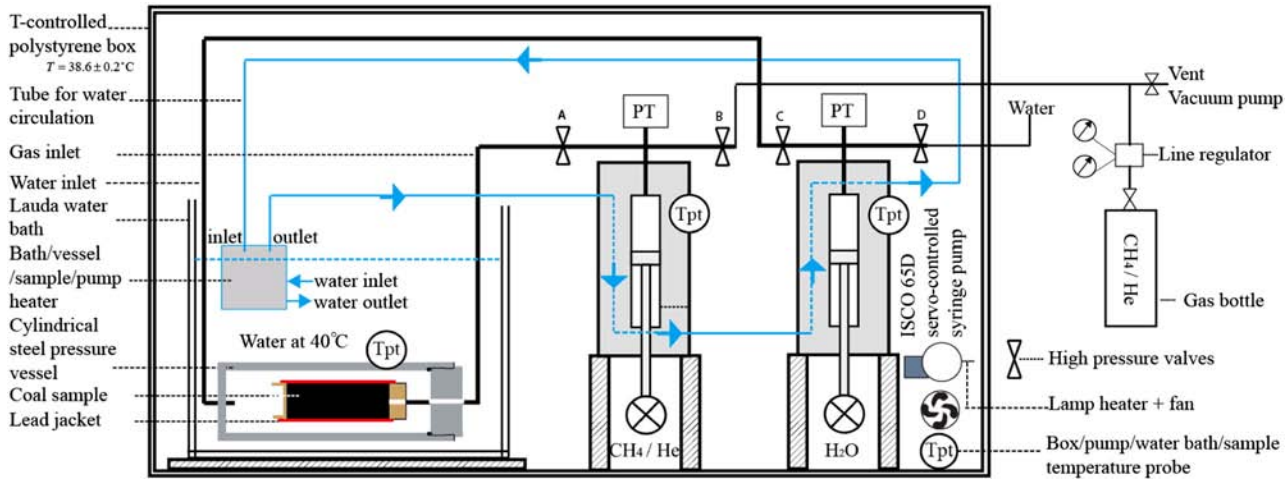

Fig. 5. Schematic illustration of the complete experimental setup. The sample, sealed in a 1 mm thick annealed lead jacket, is located inside the steel pressure vessel. The vessel is placed in the Lauda water bath at 40 ± 0.1°C. In this system, one ISCO 65D syringe pump is used for CH_4 or He pressure control within the sample, and the other for the confining pressure control. An internally heated foam-polystyrene box is constructed around the syringe pumps and water bath to control the air temperature around the setup at 38.6 ± 0.2°C.

3.1.5. Experimental procedure

We performed two experiments, Exp1 and Exp2, on the single composite sample of stacked coal discs (Fig. 4) at a constant temperature of 40°C. The following stages were employed in both experiments, as illustrated in Fig. 6.

I) Evacuation. To ensure that residual gas and water were completely removed from the sample, we evacuated the complete setup using a high vacuum pump (see Fig. 5), while the sample was subjected to a confining pressure of 3 MPa at the experimental temperature of 40°C. During this process, the sample shrank at a decreasing rate. We assumed that the sample reached equilibrium, i.e. that virtually all water was removed, when no further volume reduction could be detected by the confining pressure syringe pump. This took another 5 days. It can be expected that this high vacuum treatment at 40°C for even 5 days will be as effective in drying coal as heating it to the boiling point of water at atmosphere pressure, though we did not check this.

II) Preparatory confining pressure cycling under vacuum. To minimize any irreversible (permanent) deformation or failure of the sample during the main phase of the experiments, we then cyclically stressed the sample up to 45 MPa confining pressure, which is higher than the maximum confining pressure of 43 MPa used in the main phase of the experiments. This was achieved using the H_2O pump, while still applying a vacuum to the sample.

III) Helium expulsion test. To estimate the amount of CH_4 expelled from the free volume of the sample (i.e. non-adsorbed CH_4) by poro-elastic compaction during hydrostatic loading, helium (He), a non-sorbing gas, was used as a control gas. The He expulsion tests were conducted by first applying a confining pressure of 11 MPa and then injecting He into the sample at 10 MPa. The confining pressure was then stepped to 43 MPa following the same procedure described below for the subsequent CH_4 expulsion run, ultimately returning smoothly to 11 MPa (see Fig. 6. and point V). The duration of each confining pressure step employed using He was around 25 hours.

IV) Initial equilibration of the sample with CH_4. After venting and then evacuation of residual helium from the sample under a confining pressure of 11 MPa, we injected CH_4 at a pressure of 10 MPa. Equilibrium was assumed to be reached when the CH_4 flow rate reached a constant value, which was equal to or close to the measured pre-test leakage rate of ~12.3 μl/h (*c.f.* ~52.6 μl/h for He), and when sorption-induced swelling of the sample had stabilized. It took ~14 days to ensure that the sample equilibrated sufficiently with CH_4 at this stage. The constant flow rate of CH_4 attained at this stage was assumed to be the current leak rate. The difference between the current and pre-test leak rates is minor, and is assumed to be caused by fluctuations in system sealing capacity caused by small temperature changes and changing ISCO pump piston/seal position during our long term tests. To minimize the effects of these fluctuations on leak rate correction, the average of the current and pre-test leak rates was taken as the leak rate during the adsorption process.

V) CH_4 expulsion test. Once the sample approached equilibrium with CH_4 at the initial confining pressure, the confining pressure was increased in steps, allowing equilibrium to be reached or at least closely approached after each increment. The confining pressures used in the experiments were 16 MPa, 23 MPa, 32 MPa, and 43 MPa, generating conventional (Terzaghi) effective stress of 6, 13, 22 and 33 MPa (see Fig. 6). The pressure increase in each step was applied in less than 10 s. Around 40 hours was allowed after each step to ensure re-equilibration, i.e. to attain a constant CH_4 flow rate equal to, or at least close to, the constant flow rate attained in the previous step and in the pre-test leak calibration. Finally, the confining pressure was smoothly decreased to the initial confining pressure of 11 MPa (effective pressure of 1 MPa). Total test duration was around 10 days. Within this period, the constant CH_4 flow rates attained at each confining pressure used were slightly different, and also slightly different to the leak rate measured in the pre-test calibration. To correct for leakage at each confining pressure employed in the stepping sequence, we again took the average value of the constant CH_4 flow rates attained "before and after" each step.

VI) In addition to the above, two more CH_4 expulsion runs were performed in Exp2 only. These runs were executed directly after the CH_4 expulsion run (i.e. Fig. 6, stage V), to examine the reversibility of the CH_4 sorption/desorption process.

3.1.6. Data processing

3.1.6.1. Initial CH_4 uptake vs. associated swelling strain. The introduction of CH_4 into the sample at 10 MPa at the initial confining pressure of 11 MPa, led to an expansion of the sample measured by the ISCO H_2O pump. Now, the total amount of CH_4 entering the sample at this point consists of two components: an amount entering the free pore volume of the sample, and the amount taken up by diffusion plus adsorption in the coal matrix. The associated expansion is therefore expected to consist of a rapid poro-elastic expansion plus a time-dependent sorption-induced swelling component. Such behaviour indeed occurred (see Fig. 7). We assume that the rapid increase in the H_2O pump volume seen within ~120 seconds after the introduction of CH_4 (Fig. 7) was fully caused by the poro-elastic effect, and that sorption dominated thereafter, so that the volumes for both CH_4 and H_2O pumps at 350 s in Fig. 7 could be taken as the starting volumes for adsorption, i.e. the volume at sorption time $t = 0$. On this basis, the amount of CH_4 uptake by the sample versus time was then calculated via the expression $\Delta V(t) =$

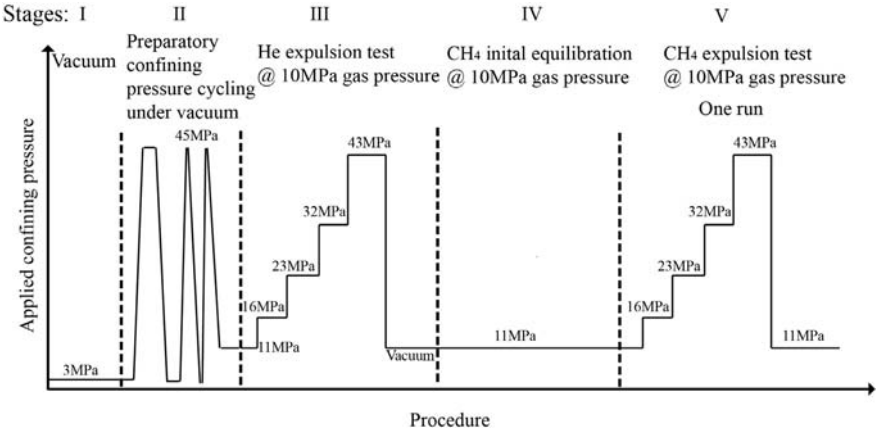

Fig. 6. Illustration of the various stages employed in the experimental procedure adopted in executing Exp1 and Exp2.

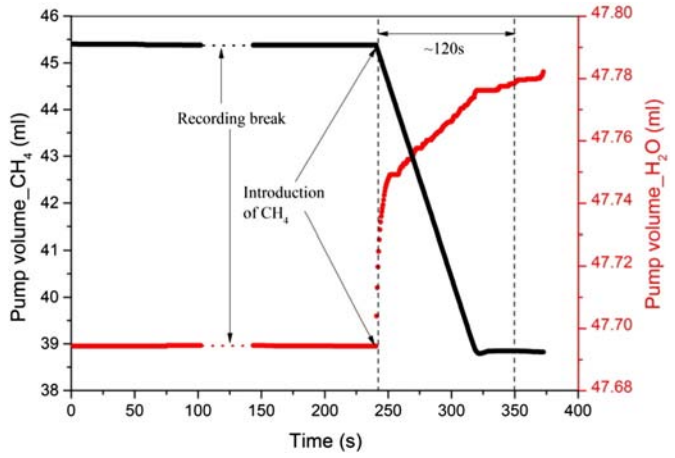

Fig. 7. The initial, short-term response of the system due to CH_4 injection into the sample at 10 MPa pressure under a confining pressure of 11 MPa, in Exp2, Stage IV. Both pumps were controlled in constant pressure mode, and their maximum flow rates were set at 5 ml/min when maintaining the constant pressure. To maintain CH_4 pressure at 10 MPa after introduction, the CH_4 pump hit the maximum flow rate of 5 ml/min.

$V^{start} - V(t) - Qt$. Here $V(t)$ (ml) represents the pump volume for CH_4 at time t, V^{start} (ml) represents the corresponding starting pump volume for CH_4, Q represents the leak rate (ml/hour) of the pump, and t (hours) represents elapsed adsorption time. We took the average value of ΔV over the final 5 hours of the initial equilibration interval as the total amount of gas uptake by the sample at equilibrium within that interval. To obtain the concentration of CH_4 (mol/kg_{coal}) taken up by the sample versus time, after initial introduction of CH_4 at 10 MPa pressure, we used the relation $C(t) = \frac{\Delta V(t)\rho_{CH_4}}{m}$, where ρ_{CH_4} is the density of CH_4 at 10 MPa pressure and 40°C expressed in mmol/ml, and m (g) is mass of the coal sample.

The associated (positive) volumetric swelling strain of the sample measured due to CH_4 adsorption was calculated using the relation $e_{\bar{v}}^{ads}(t) = (\Delta V_{H_2O}(t)/V_{sample}) \cdot 100\%$, where $\Delta V_{H_2O}(t)$ is the volume change of the H_2O pump referred to the start of adsorption (i.e. the volume of the H_2O pump shown in Fig. 7 at 350 s), and V_{sample} is the initial volume of the sample under unconfined conditions, which was measured before the experiments. Again, we took the value of $e_v^{ads}(t)$ over the final 5 hours of the initial equilibration interval as the total swelling strain (e_{ads}^{eq}) of the sample caused by CH_4 adsorption at equilibrium within that interval.

3.1.6.2. CH_4/He expulsion. The amount of CH_4/He leaving the sample in response to each confining pressure step i versus time was calculated via the expression $\Delta\overline{V}_i(\Delta t_i) = V_i^{Pump}(\Delta t_i) - V_i^{start} + Q\Delta t_i$. Here, $\Delta\overline{V}_i$ (ml) is measured such that CH_4/He expulsion is taken as positive, $V_i^{Pump}(\Delta t_i)$ (ml) represents the internal gas pump volume during the confining pressure interval i, V_i^{start} (ml) represents the starting pump volume at the initiation of confining pressure step i, Q represents the leak rate (ml/hour) of the pump during each confining pressure interval i, and Δt_i represents elapsed time (hours) during the ith applied pressure interval referred to the starting time of each step. Again, we took the value of $\Delta\overline{V}_i$ over the final 5 hours of the current confining pressure step as the amount of gas expelled from the sample at equilibrium in response to the current increment of confining pressure. The total CH_4/He expulsion over j consecutive steps was hence calculated using $\Delta\overline{V}_j = \sum_1^j \Delta\overline{V}_i$.

3.1.6.3. Error analysis. Uncertainty in the amount of CH_4/He expulsion calculated using the methods described above was caused by 1) the noise on the pump volume signal due to the control accuracy in pressure control mode, and 2) slight differences in leak rate of the CH_4/He pump in each step. We analyze the uncertainty caused by each of these independently, using the standard deviation (SD) expressed as $\eta = \sqrt{\frac{1}{n}\sum(\bar{x}_i - x_i)^2}$ for data set X consisting of n data points. We took the largest error as the uncertainty in CH_4/He expulsion data. The biggest error for CH_4 expulsion data resulted from fluctuations in leak rate during long duration experiments (40-50 hours for each confining pressure step), while for He expulsion data resulted from the noise due to high compressibility of He.

3.2. Results

3.2.1. CH_4 uptake and swelling response during initial pressurization with CH_4

CH_4 uptake and the associated volume changes exhibited by the single composite sample during initial equilibration at a CH_4 pressure of 10 MPa and at a confining pressure of 11 MPa, in Exp1 and Exp2, are plotted as a function of time in Fig. 8. In both cases, equilibration took ~190 hours. The CH_4 uptake by the sample is seen to lie in the range of 6.33-6.47 ml, while the corresponding volumetric swelling is 0.368-0.399 ml, which means an equilibrium swelling strain of 1.29-1.39%. The density of the CH_4 at 10 MPa and 40°C is 4.3651 mmol/ml (Setzmann and Wagner, 1991), which in turn means that the CH_4 uptake of the sample at equilibrium is 0.799-0.816 mol/kg_{coal}. The uptake of CH_4 ($C(t)$) expressed in mol/kg_{coal} is plotted against the measured volumetric swelling strain ($e_v^{ads}(t)$) in Fig. 9. The volumetric swelling strain developed close to linearly with CH_4 uptake during initial equilibration at constant confining pressure of 11 MPa and 10 MPa CH_4 pressure.

3.2.2. He and CH_4 expulsion data (confining pressure stepping)

The total amount (ml) of He and CH_4 expelled from the sample at equilibrium versus the applied confining pressure for both experiments (i.e. for Exp1 and Exp2) are presented in Fig. 10a. An increase in expulsion of both CH_4 and He is clearly seen in Fig. 10a as a result of upward confining pressure stepping. At 43 MPa confining pressure, i.e. 33 MPa effective stress, ~0.59 ml (average) CH_4 and ~0.2 ml (average) He are expelled from the sample. The data trends for both CH_4 and He are near-linear in the interval 16-43 MPa, but show a non-linear region in the interval 11-16 MPa. Moreover, Fig. 10b illustrates the amount of expelled CH_4 (ml) versus time during the three CH_4 expulsion runs performed in Exp2 (i.e. the run shown in stage V in Fig. 6 plus the two additional runs of stage VI). This indicates that transfer of CH_4 from/

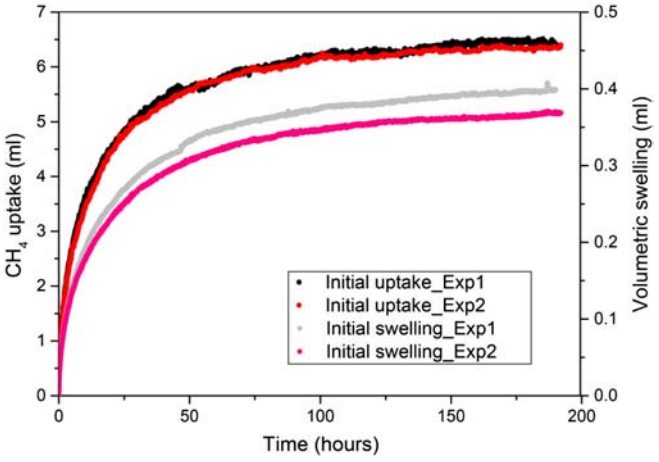

Fig. 8. CH_4 uptake/swelling versus time during initial isothermal equilibration of the Brzeszcze coal sample (disc stack) subjected to a confining pressure of 11 MPa with CH_4 pressure of 10 MPa (Stage IV of Exp1 and Exp 2). The swelling (ml) was obtained from the volume change of the H_2O pump, while the CH_4 uptake (ml) was derived from both volume change and leakage rate of the CH_4 pump.

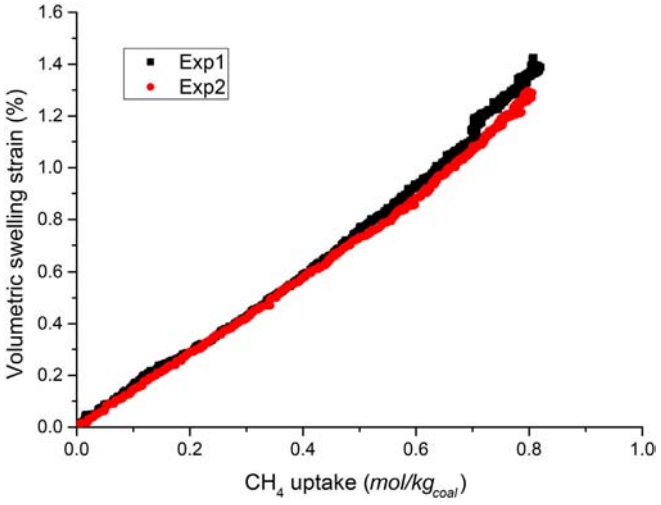

Fig. 9. Total volumetric swelling strain versus total CH_4 uptake of the Brzeszcze sample (disc stack) during initial equilibration in Stage IV of Exp1 and Exp2 at a CH_4 pressure of 10 MPa and at a confining pressure of 11 MPa at 40°C (see Fig. 8).

into the sample caused by the change in confining pressure was reversible in Runs 2 and 3, though irreversible in Run1.

4. Discussion

Our experiments show that the equilibrium CH_4 uptake by the Brzeszcze high volatile bituminous coal (5.2% ash content), at 40°C, at a pressure of 10 MPa, and under a confining pressure of 11 MPa, is 0.799-0.816 mol/kg_{coal}. This is similar to the value of 0.626 mol/kg_{coal} obtained by Busch (2005) for the sorption capacity of similar coal (17.03% ash content) from the Brzeszcze mine, measured unconfined at 10 MPa CH_4 pressure at 45°C. The sorption-induced volumetric swelling strain measured in the present experiments was 1.29-1.39%, which is also in good agreement with the volumetric swelling strains of 1.07-1.96% measured for Bituminous Coals A and I by Day et al. (2010). More importantly, our experiments demonstrate that increasing the hydrostatic confining pressure resulted in CH_4 being expelled from the solid sample in excess of helium expulsion (see Fig. 10a). This means the CH_4 indeed desorbed from the coal matrix due to application of the hydrostatic stress, which is consistent with our model prediction.

In the following, we compare our experimental data with our theory for sorption under stress. We start by determining the partial molar volume (V_0) of the adsorbed CH_4 using our experimental data on CH_4 uptake vs. associated swelling strain. We go on to calculate the amount of CH_4 truly desorbed from the sample using the CH_4 and He expulsion data. We subsequently compare the CH_4 capacity of the sample under stressed conditions, derived from the experimental data, with our model. Finally, we apply our modified model to predict in-situ CBM content.

4.1. Experimental data versus theory

4.1.1. V_0 determination

The linear relation between CH_4 uptake ($C(t)$) and associated volumetric swelling strain ($e_v^{ads}(t)$) shown in Fig. 9 indicates that the measured volumetric swelling strain is caused by adsorption of CH_4, and that this relation can be expressed as $e_v^{ads}(t) = \rho V_0 C(t)$ in line with

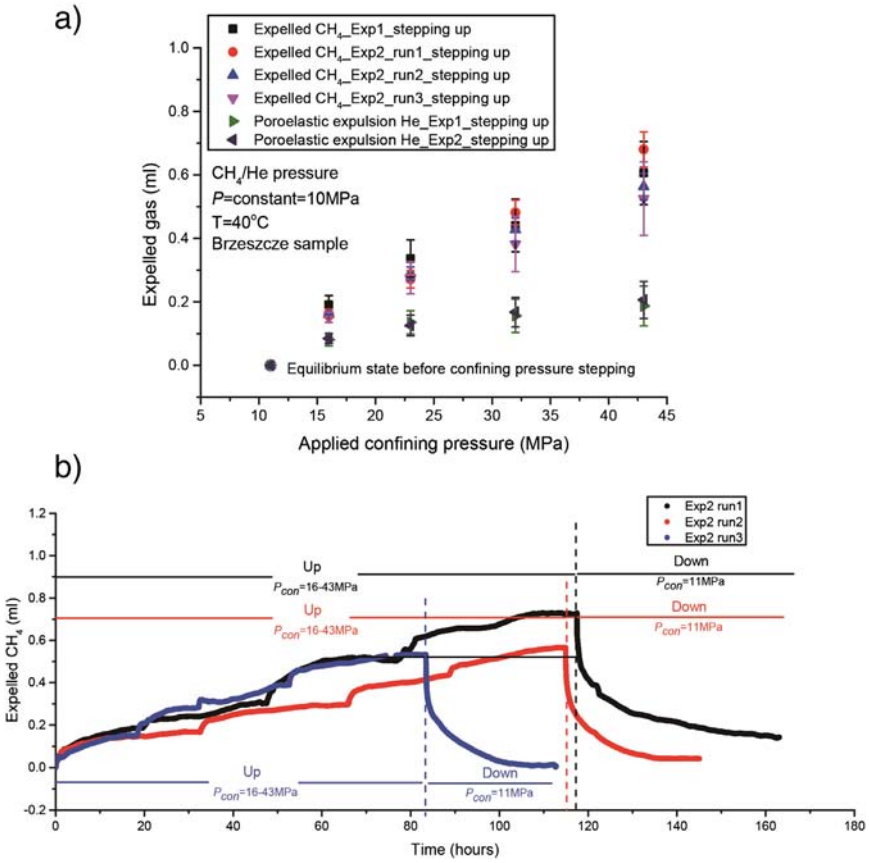

Fig. 10. CH_4/He expulsion data. a) The absolute amount of CH_4/He expelled from the Brzeszcze coal sample (disc stack) at equilibrium, as a function of confining pressure applied after initial equilibration of the sample at a confining pressure of 11 MPa with CH_4/He pressure of 10 MPa. b) Expelled CH_4 from Brzeszcze sample (disc stack) versus time during the three runs conducted in Exp2.

our model (Hol et al., 2012a; Hol and Spiers, 2012), with V_0 being independent of the adsorbed concentration ($C(t)$). We obtained the value of V_0 from a best fit of the above expression to the experimental data shown in Fig. 9, which yields 1.40-1.46 $\times 10^{-5}$ m^3/mol for the volume change of the sample due to adsorption of one mole of CH_4. This result is consistent with values (i.e. e_v^{ads}/C) of 1 to 2×10^{-5} m^3/mol reported for CH_4 in the literature (Day et al., 2010; Hol et al., 2011, 2012a; Hol and Spiers, 2012; Levine, 1996; Pan and Connell, 2007).

4.1.2. Truly desorbed CH_4

The expelled CH_4 data shown in Fig. 10a represent the combined effects of expulsion due to poro-elastic compression plus any stress-induced desorption, i.e. desorption from the solid sample caused by the effect of hydrostatic confining pressure. Under the assumption that all He-accessible pores were filled with free CH_4, the amount of CH_4 truly desorbed from the sample ($C_{des}^{CH_4}$) was calculated using the expression $\left(C_{des}^{CH_4}\right)_i = \left[s\left(\Delta\overline{V}_i^{CH_4}\right) - s\left(\Delta\overline{V}_i^{He}\right)\right]\cdot\rho_{CH_4}$. Here $s\left(\Delta\overline{V}_i^{CH_4}\right)$ and $s\left(\Delta\overline{V}_i^{He}\right)$ represent the average volumes of CH_4 (four data points) and of He (two data points) expelled at the *ith* confining pressure shown in Fig. 10a, while ρ_{CH_4} is the density of CH_4 (4.3651 mmol/ml) at a pressure of 10 MPa and at 40°C (Setzmann and Wagner, 1991). For each average in the above expression, the standard derivation (SD) was taken as the uncertainty in each quantity.

The truly desorbed amounts of CH_4 obtained, expressed as $C_{des}^{CH_4}$ in mol/kg$_{coal}$ and as a percentage (%) of the initial uptake of 0.808 mol/kg$_{coal}$ (average) at the confining pressure of 11 MPa, are plotted versus applied confining pressure in Fig. 11a and b. An essentially linear increase in desorption is clearly seen in Fig. 11, in direct proportion to upward confining pressure stepping. This implies that the non-linear region observed in the interval 11-16 MPa in Fig. 10a, for both CH_4 and He, resulted from the closure of cracks and the gaps between the discs of the sample upon loading. At 43 MPa confining pressure, i.e. 33 MPa effective stress, about 0.05 mol/kg$_{coal}$ of CH_4 is desorbed from the sample (Fig. 11a), which corresponds to a reduction of ~6.2% in the initial uptake (Fig. 11b).

This reduction, caused by the positive effective stress applied in our experiments, is much smaller than that (>85%) reported by Pone et al. (2009) for solid (not composite) samples of cylindrical bituminous coal (25 mm in diameter). This suggests that the large reduction in CH_4 sorption capacity reported by Pone et al. (2009) is probably not due solely to a direct effect of stress on equilibrium sorption capacity, but also to a reduction in the volume of coal sample that was accessible to CH_4 as sample permeability decreased with increasing confining stress.

4.1.3. Comparison with present model for stressed coal

Strictly speaking, the truly desorbed CH_4 (i.e. in excess of He poroelastic expulsion) shown in Fig. 11a should be referred to as the change in excess sorption capacity, while the change in absolute sorption capacity cannot be directly measured from the experiments. However, since our model considers coal matrix material which contains nanopores only, it treats the adsorbed gas molecules as being a "dissolved" component of the solid phase (following Myers, 2002), as opposed to assuming an independently identifiable adsorbed phase. This means that the excess sorption capacity in our model should equal the absolute sorption capacity.

To compare our results with our thermodynamic model as written in Eqs. (28a) and (28b), we first convert the truly desorbed CH_4 ($C_{des}^{CH_4}$) into the sorption capacity (uptake, C) at the *ith* applied hydrostatic stress via the expression $C_i = C_0 - (C_{des}^{CH_4})_i$. Here C_0 is the average of the initial uptake that we measured during Exp1 and Exp2 at a confining pressure of 11 MPa and at 10 MPa CH_4 pressure. The data points with the calculated error bars are shown in Fig. 12. Taking a thermodynamic reference state defined at $P = 0.1$ MPa, we then determined the CH_4 activity (a_g) to be 87.58 at a pressure of 10 MPa and 40°C (Setzmann and Wagner, 1991). Our model (Eq. (28)) was subsequently fitted to our data (Fig. 12) under the assumption that the partial molar volume of the adsorbed gas molecule V_0 is insensitive to the stress state. Taking the average value of V_0 obtained from the $e_v^{ads}(t)$ vs. $C(t)$ data shown in Fig. 9 to be 1.43×10^{-5} m^3/mol, the best fit of the model (Eqs. (28a) and (28b)) to our data ($R^2 = 0.994$) shown in Fig. 12 gave the parameters $C_s = 1.219$ mol/kg and $K^0 = 0.0235$ obtained fitting Eq. (28a), versus $C_s = 1.219$ mol/kg and $K = 0.0223$ obtained fitting Eq. (28b). This difference in K^0 versus K points to the effect of gas pressure on μ_s^P (see Eqs. (5a), (5b) and (5c)) and hence on K. Alternatively, the thermodynamic equilibrium constant $K^0 = 0.0235$ can be obtained using Eq. (23), by inserting the value of K (0.0233) retrieved from fitting Eq. (28b) to our data, along with the constant CH_4 pressure of 10 MPa that was employed in all experiments.

Note that the parameter values (C_s, K^0) obtained by fitting Eq. (28a) are independent of gas pressure and stress state, and so can be applied for all gas pressures and stress states. The parameter values (C_s, K) obtained fitting Eq. (28b) are also independent of stress state but depend on gas pressure. These parameters, C_s and K in Eq. (28b), can be identified with the Langmuir constants (C_L, K_L, see Section 2.5). and their values (C_s, K) obtained by fitting Eq. (28b) fall within the range of

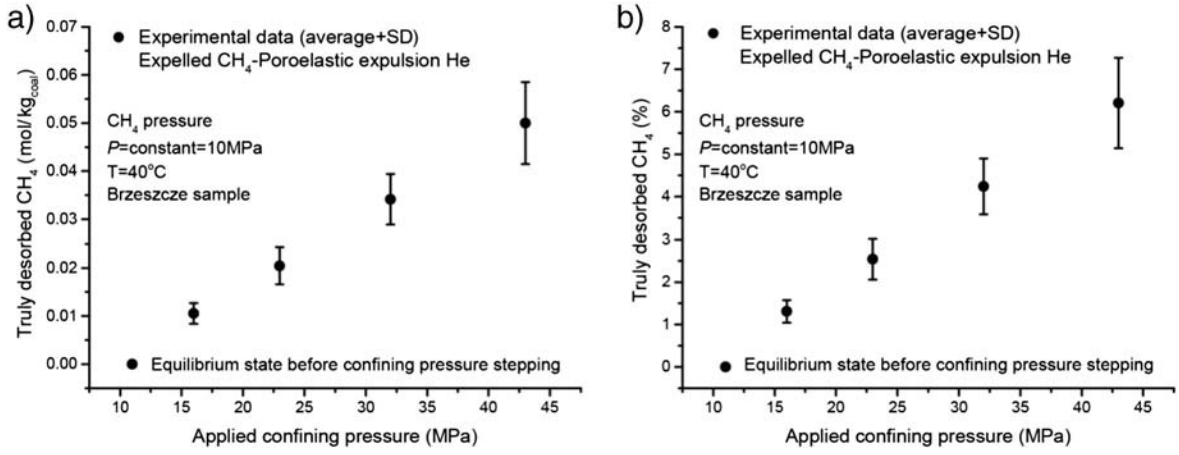

Fig. 11. Truly desorbed CH_4 at equilibrium, averaged for all experiments/runs, versus the applied confining pressure after initial equilibration of the sample at a confining pressure of 11 MPa with CH_4 pressure of 10 MPa. The mean data point values plus standard deviation (SD) shown were derived from the experimental data shown in Fig. 10a, by means of standard statistical analysis. (a) shows absolute amount of CH_4 truly desorbed per applied confining pressure step, expressed in mol/kg$_{coal}$. (b) shows the truly desorbed amount of CH_4 as a percentage (%) of the uptake value of 0.808 mol/kg$_{coal}$ (average) at initial equilibrium before increasing the confining pressure.

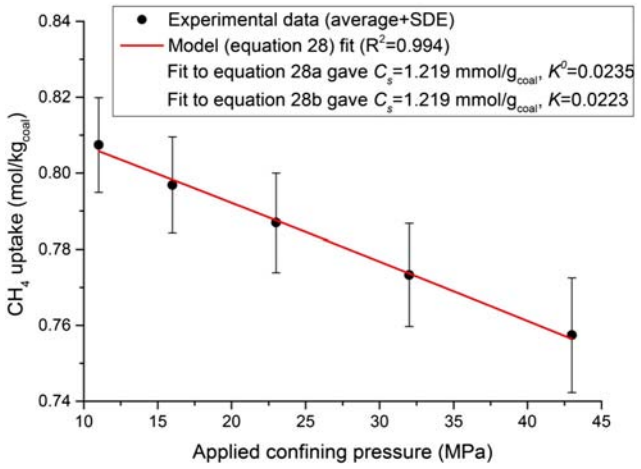

Fig. 12. CH_4 uptake versus applied confining pressure. The black dots represents CH_4 sorption capacity derived from our experimental data expressed in mol/kg_{coal}, and the red line represents the best fit of our thermodynamic model (Eqs. (28a) and (28b)).

Langmuir constants ($0.9 \le C_L \le 2.5$ mol/kg_{coal} and $0.02 \le K_L \le 0.05$) reported in the literature for unstressed, high volatile bituminous coal, i.e. our values for C_s and K fall within the range obtained from best fitting of the classical Langmuir equation to isothermal CH_4 sorption data (e.g. Cui et al., 2007; Dutta et al., 2011; Gensterblum et al., 2013; Laxminarayana and Crosdale, 1999; Levine, 1996; Merkel et al., 2015; Pan and Connell, 2007; Pini et al., 2010). The quality of fit obtained in Fig. 12, and the similarity between our C_s and K values versus C_L and K_L in the literature, indicate that our model successfully describes adsorption under stressed conditions.

4.1.4. Magnitude of the stress effect for CH_4 and comparison with CO_2

The experiments reported here have shown at least a ~6% reduction in CH_4 sorption capacity of Brzeszcze coal due to the application of 33 MPa effective hydrostatic stress for a CH_4 pressure of 10 MPa at 40°C. Moreover, our results support the applicability of our model. Considering this, the deviatoric stress term in Eqs. (25a) and (25b) means that a ~6% reduction may even be an underestimate of the reduction when coal is subjected to a general stress state σ_{ij}. Crucially, the effect of stress on adsorption strongly depends on the partial molar volume V_0 of the adsorbed gas species (*c.f.* Eqs. (25a) and (25b)). In this context, the higher value of V_0 (*i.e.* $V_0 = N_A\Omega_0$) for CH_4, for a given coal type, the lower the sorption capacity at the same stress state. Conversely, if V_0 is negligible, i.e. $V_0 \to 0$, the effect of stress on sorption capacity would disappear.

In similar experiments using CO_2, Hol et al. (2012a) measured CO_2 expulsion from the high volatile bituminous coal from Brzeszcze at a constant CO_2 pressure of 15 MPa, at a temperature of 40°C, varying the confining pressure from 16 MPa to 40 MPa. They found that 0.11 mol/kg_{coal} of CO_2 was expelled from the sample at an effective confining pressure of 25 MPa, of which 0.001-0.021 mol/kg_{coal} was estimated to be due to poro-elastic expulsion. This corresponds to a 6.5-8% reduction in CO_2 sorption capacity at the effective confining pressure of 25 MPa, implying that the sorption capacity of Brzeszcze high volatile bituminous coal is similarly sensitive to the effect of stress for both CO_2 and CH_4. This is consistent with the similar values of V_0 determined for sorption of CO_2 by the Brzeszcze coal, as determined by Hol et al. (2012a). Independently of the magnitude of V_0, it is important to note that selective sorption of CH_4 or CO_2 from a CH_4-CO_2 mixture (*c.f.* Liu et al., 2015) by Brzeszcze coal, as modelled by Liu et al. (Liu et al., 2015), is unaffected by stress state. This is because the parameters C_s, K, K^0 in the present model, and the equivalent parameters C_s and K in the models presented by Liu et al., are independent of stress state.

4.2. In-situ CBM content predicted by our model

Our experimental results and our model both confirm that the in situ CBM content is determined not only by geological factors generally accounted for, such as coal rank, coal composition, moisture and temperature, but also by another important geological factor, in-situ lithostatic stress state, which is usually ignored. To evaluate the magnitude of the lithostatic stress effect by comparison with the results predicted by our model for unstressed coal expressed in well-know Langmuir form, i.e. Eq. (27b), we now proceed to apply our model expressed in Eq. (25b) to give a general prediction for CBM content distribution with burial depth.

To do that, we first need to calculate the values of parameters (C_s, K, V_0) for a given coal at different burial depths, i.e. at different temperatures. We focus on high volatile bituminous coal, for which the parameters at 40°C are known from our experiments. Beside this, we consider only dry conditions, though sorption capacity decreases with moisture content (Busch and Gensterblum, 2011; Gensterblum et al., 2013, 2014; Merkel et al., 2015; Weniger et al., 2012). We consider only dry conditions because our present model is only valid for pure gas adsorption, i.e. not valid for CH_4 and water vapor mixtures. The potential effects of water are similarly ignored in essentially all previous adsorption modeling and model fitting studies on coal (Day et al., 2008, 2011; Gensterblum et al., 2013, 2014; Merkel et al., 2015; Weniger et al., 2012), but should be evaluated in future.

Returning to the issue of temperature dependence, we start with the quantity K (Eq. (22)). From Eqs. (4), (7) and (22), μ_s^P, μ_{g0}, K are all the function of temperature, though μ_s^P also weakly depends on gas pressure. We assume that the quantity K can be mathematically expressed as $K = B\exp(DT)$, where B and D are constants, hence capturing the form of the expected T-dependence of K. We fitted this to describe the temperature dependence of K values obtained by fitting Eq. (27b) to the isothermal sorption (absolute) data obtained for high volatile bituminous coal (dry) at different temperatures by Gensterblum et al. (2013). This yielded $D = -0.03$ ($R^2 = 0.92$). Inserting the value of K at an absolute temperature of 313K (40°C) as obtained from our present experimental data (i.e. inserting $K_{313} = 0.0233$), we obtain $B = 267.4$. The quantities C_s and V_0 are assumed to be insensitive to temperature, and are consequently set at the values obtained in the present experiments, i.e. at $C_s = 1.219$ mol/kg and $V_0 = 1.43 \times 10^{-5}$ m^3/mol.

Based on bottom hole temperature of exploration wells, plus mud weight information from exploration drilling for coal in the Carboniferous of the Ruhr Basin in Germany, Freudenberg et al. (1996) estimated a geothermal gradient of 0.032°C/m, and a methane pressure gradient of 0.0097 MPa/m. We follow Freudenberg et al. (1996) in assuming these gradients. A lithostatic stress gradient of 0.025 MPa/m was taken, under the assumption that the overlying rock mass determines to the vertical stress, and that the average density of rock is 2500 kg/m^3. For simplicity, we assume that coal seams experience a hydrostatic stress, i.e. $\sigma = \sigma_{vertical}$. The CBM concentration at equilibrium was then calculated both via Eq. (27b) without considering the stress effect, i.e. using a conventional Langmuir-type model written in terms of gas activity, and via Eq. (28b) considering the additional effect of the in-situ stress (assumed hydrostatic).

The resulting model predictions for CBM concentration and its reduction compared with conventional predictions are plotted as a function of depth in Fig. 13. The results illustrate that 1) the highest in-situ CBM concentration predicted by Eq. (28b) occurs at a burial depth of ~900m, which is 75m shallower than that predicted by Eq. (27b); 2) the highest in-situ CBM concentration predicted by Eq. (28b) yields a value of 0.76 mol/kg_{coal}, which is 2.9% lower than that predicted by Eq. (27b); 4) the deeper the coal seam, the more significant the effect of stress; 5) a ~6% reduction in CBM content occurs at a depth of ~1800m compared with that predicted by Eq. (27b).

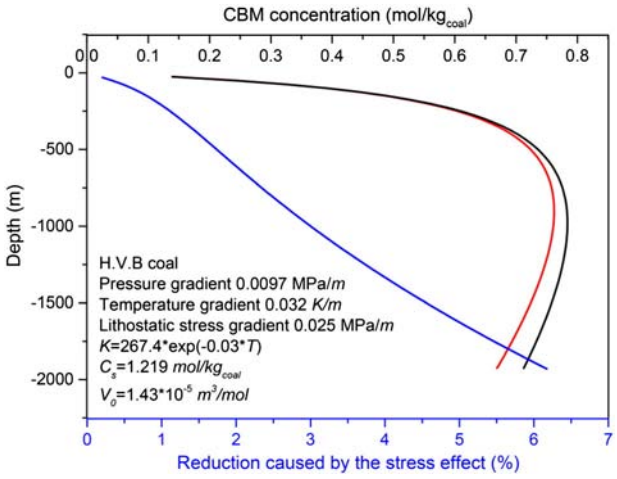

Fig. 13. Model predictions of equilibrium CBM content for dry high volatile bituminous coal as a function of depth. The gas pressure, temperature and lithostatic stress gradients used in the model were derived from Freudenberg et al. (1996), while K, C_s and V_0 were based on the present experimental results and those of Gensterblum et al. (2013) (see text). The black line represents the methane content concentration predicted by Eq. (27b) without considering the effect of in-situ stress, while the red line predicted by Eq. (28b) considering the in-situ stress effect. The blue line represents the reduction (%) in CBM content concentration caused by the effect of in-situ stress.

5. Implications for (E)CBM

Our results have confirmed that the in-situ lithostatic stress can reduce the CH_4 sorption capacity of coal, and imply a reduction in the prediction of the CBM content compared with those made using the Langmuir type isotherm applied for unconfined conditions. This finding has the following implications for (E)CBM.

5.1. Effect of lithostatic stress on CBM saturation and its impact on production

Coal is generally believed to be under-saturated with methane in-situ, i.e. CBM content is lower than the sorption capacity of unstressed coal measured at in-situ *P-T* conditions (Moore, 2012). The reasons for this given by Moore (2012) are a) gas is expelled or leaks from coal during uplift, and b) gas is stripped from coal by moving water. The level of gas saturation plays a significant role in assessment of CBM production (Moore, 2012). This is generally calculated by comparing the gas desorbed from coal samples recovered in a sealed the canister, i.e. in-situ gas content ($C_{in\text{-}place}$), with the sorption capacity measured by determining the adsorption isotherm for the unstressed sample at the correct *P-T* conditions ($C_{unstressed}$) (Mares et al., 2009; Moore, 2012).

However, our results clearly indicate that the in-situ stress reduces CH_4 sorption capacity compared with that for unstressed coal measured at given *PT* conditions in laboratory. This means that if gas saturation is calculated via the conventional methods given by Moore (2012) described above, i.e. as $C_{in\text{-}place}$ / $C_{unstressed}$, the reduction in sorption capacity caused by the lithostatic stress also contributes to in-situ CBM content being apparently under-saturated. This further suggests that the true gas saturation, calculated from in-situ gas content over the sorption capacity for stressed coal ($C_{stressed}$), i.e. from $C_{in\text{-}place}$ / $C_{stressed}$ (not from $C_{in\text{-}place}$ / $C_{unstressed}$), should provide an indicator of the real loss of gas in coal seams. At the same time, variation in spatially distributed measurements of the gas content in place in a coal seam might be in part due to spatial variation in the stress state.

The effect of lithostatic stress on gas saturation for CBM productions is illustrated in Fig. 14. Taking Brzeszcze high volatile bituminous coal as an example, and assuming that in situ temperature is 40°C at a burial depth of around 1200 m, we plotted sorption capacity under a given in-situ stress state as a function of methane pressure (i.e. using Eqs. (27b) and (28b)). We assume that in-situ gas content concentration for Brzeszcze high volatile bituminous coal at a depth of 1200 m is only 70% of the maximum sorption capacity for unstressed coal at corresponding *PT* conditions (Fig. 14a), i.e. we assume 70% conventional gas saturation. In practice, gas cannot be recovered until the reservoir is depressurized (i.e. de-watered) to a pressure of P_c, which is commonly referred to as critical desorption pressure (Moore, 2012). The conventional model for unstressed conditions (Eq. (27b)) predicts that P_c, in Fig. 14a, is 5 MPa, while the model for stressed conditions (Eq. (28b)) predicts that is 6 MPa. This means a reduced time for triggering of gas production under in-situ conditions (stressed), than that typically expected based on adsorption isotherms for unstressed coal. Conversely, as illustrated in Fig. 14b, a lower amount of gas would be produced at the in-situ stress state for a fixed critical desorption pressure P_c than expected on the basis of conventional sorption data for unstressed coal.

5.2. Effect of lithostatic stress on coal seam permeability

During (E)CBM production, ad/desorption of gas species such as CO_2 and CH_4 causes swelling/shrinkage of coal, hence leading to changes in stress state and inevitably in cleat permeability under in situ conditions where displacements are constrained (Espinoza et al., 2014; Liu et al., 2011; Pan and Connell, 2012). The change in stress state also results in changes in the ad/desorption process. This fully coupled stress-strain-sorption behavior of coal can be captured by inserting the revised model developed in this paper into the constitutive model proposed by Hol et al. (2012a). The modified constitutive model is formulated as

$$\varepsilon_{ij}^{eq} = \varepsilon_{ij}^{poro} - \frac{V_0\rho(A_{ij}+\delta_{ij})}{3}C \tag{29}$$

where ε_{ij}^{eq} represents the total strain, ε_{ij}^{poro} represents the anisotropic elastic properties on the scale of the REV expressed by the poro-elastic equation (Biot, 1941; Wang, 2000), and $\frac{V_0\rho(A_{ij}+\delta_{ij})}{3}C$ represents the swelling/shrinkage of the coal matrix caused by adsorption of gas species expressed through Eqs. (25a) and (25b). Note here that compressive stress and strain are positive. This full coupling of stress, strain and sorption offers an important tool for modeling permeability evolution during (E)CBM. Its implications for (E)CBM, especially for permeability evolution during (E)CBM production are beyond the present scope and are reserved for a future reservoir modeling study.

5.3. Suggestions on strategies of (E)CBM production and CO_2 sequestration in coal seams

Our sorption model for a general stress state (Eqs. (25a) and (25b)) clearly shows that the equilibrium concentration of gas adsorbed by coal is a function of gas pressure, stress state, and the temperature. This, combined with poro-elastic deformation as described by Eq. (29), offers a theoretical basis for developing new techniques making use of the effect of in-situ stress, temperature and gas pressure on gas sorption, which can potentially be applied in (E)CBM production. For example, if there is a CH_4-rich coal seam that been partially mined, the gradient in stress state between the mined and unmined regions will provide an additional driving force, in excess of the gradient in gas pressure and concentration, for CH_4 flow from the unmined coal to the mined region. In such cases, a coal seam that has been partially mined, or where the stress state has been otherwise perturbed, might perhaps become more gas productive. Moreover, our model offers an improved tool for estimating the amount of CO_2 that can be adsorbed by coal seams or can be sequestrated in coal seams at given injection pressure, stress state and temperature.

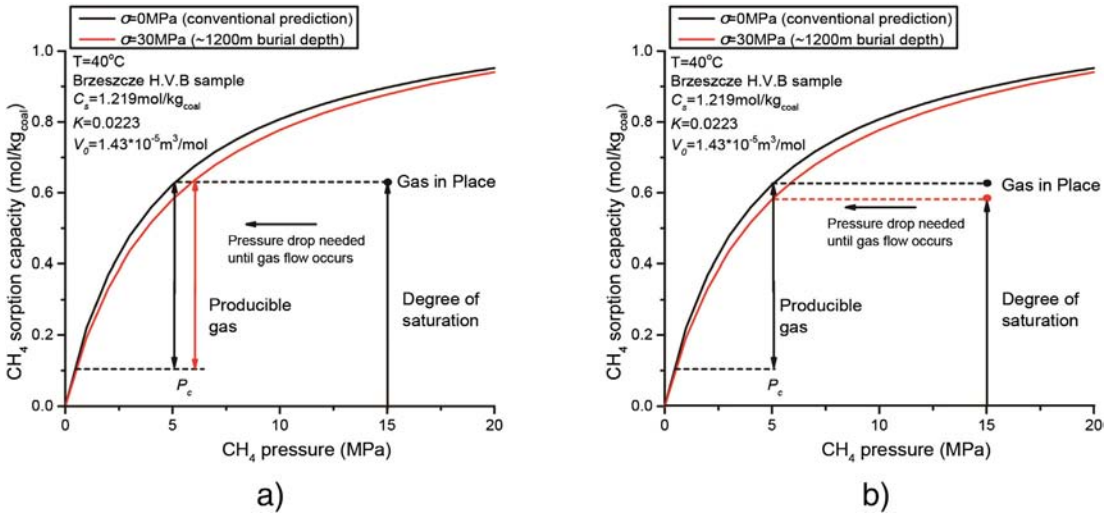

Fig. 14. Effect of in-situ stress on gas production assuming Brzeszcze high volatile bituminous coal with a given gas saturation. a) for the same gas saturation and b) for the same critical desorption pressure P_c.

6. Conclusions

The main findings and conclusions of this study are summarized as follows.

1. A corrected model for adsorption of any pure gas species by coal under stressed conditions has been derived. In the present model, the true equilibrium constant K^0 for sorption is expressed through the standard free energy change $(\mu_s^{P_0}(T) - \mu_{g0}(T))$, which depends only on temperature for a given coal and gas/fluid species. Our model demonstrates that an applied effective stress reduces the gas sorption capacity of coal and that the magnitude of the reduction depends on the partial molecular volume (Ω_0) of the adsorbed molecule.
2. To test our thermodynamic model, and specifically to test the effect of stress on the CH_4 sorption capacity of coal, we performed experiments on a single composite coal sample (Brzeszcze 364 high volatile bituminous coal) containing artificially introduced transport paths, which minimized the influence of the positive Terzaghi effective stress on sample permeability and hence accessibility of the sample to CH_4. The amount of CH_4 expelled from the sample was measured by increasing the hydrostatic stress or confining pressure in the range 11-43 MPa, after initial equilibration of the sample with CH_4 at a fixed methane pressure of 10 MPa and at a fixed temperature of 40°C. The true amount of CH_4 desorbed from the sample was obtained by subtracting the poro-elastic gas expulsion determined by means of helium (a non-sorbing gas) control experiments. The results show that about 0.05 mol/kg$_{coal}$ of CH_4 desorbed from the solid sample when the applied confining pressure increased from 11 MPa to 43 MPa, which corresponds to ~6.2% of the initial uptake of 0.808 mol/kg$_{coal}$.
3. The present model describes our experimental data well. The results indicate that our model successfully captures the physical process of gas adsorption by coal that supports a stress state applied in excess of the pressure of the sorbing gas species.
4. We apply our model to predict the in-situ CBM concentration distribution with depth for dry, high volatile bituminous coal, for an assumed geothermal gradient of 32°C/km. The results indicate a maximum CH_4 concentration of ~0.76 mol/kg$_{coal}$ at a burial depth of ~900 m, which is ~3% lower than conventional predictions made without considering sorption-induced swelling and hence the effect of stress. This reduction is minor but helps to explain why gas saturation is generally lower than expected from conventional sorption measurements on unconfined coal powders. More importantly, our results confirmed that there is an intimate coupling between in-situ stress, strain and sorption in coal that needs to be considered in gas-enhanced CBM strategies.

Acknowledgements

The China Scholarship Council (CSC) and Total S.A. are gratefully acknowledged for their financial support of first author Jinfeng Liu and of the research project. Sander Hol is also thanked for discussions and help in understanding his model and the experimental apparatus at Utrecht in the early stages of this project.

Appendix A. Statistic mechanics approach to obtaining sorbed concentration under stress

A.1. Canonical partition function for adsorption of n molecules

For a total population of adsorption sites n_s (fixed), we assume that each adsorption site remains empty or else takes up one gas molecule, and that there is no interaction between adsorbed molecules. When n molecules are adsorbed (where $n < n_s$), the canonical partition function for the solid system is written (Hill, 2012)

$$Q(n_s, n, T) = q(\sigma_{ij}, T)^n \frac{n_s!}{n!(n_s - n)!} \tag{30}$$

The term $\frac{n_s!}{n!(n_s-n)!}$ is the degeneracy factor or the number of the ways W' in which the n molecules can be arranged in the n_s adsorption sites. The term q is the partition function for one single adsorbed molecule in the stressed solid, written

$$q = \exp\left[\frac{-\mu_s^{\sigma}}{kT}\right] \tag{31}$$

where quantity μ_s^{σ} represents chemical potential of one adsorbed molecule under stressed conditions (see Fig. 2), as given by Eq. (5b)

A.2. Chemical potential per molecule for n molecules adsorbed by stressed coal

In line with standard statistical mechanics theory, the chemical potential per molecule for n adsorbed molecules is given as

$$\mu_s = kT\left(\frac{\partial \ln Q}{\partial n}\right) \tag{32}$$

Applying Stirling's approximation $\ln x! \approx x(\ln x - 1)$ for large x to the above expression (32), we obtain

$$\mu_s = kT\left(\ln\frac{n}{n_s - n} - \ln q\right) = kT\ln\frac{\theta}{1-\theta} + \mu_s^{\sigma} \tag{33}$$

where $\theta = \frac{n}{n_s}$. Eq. (33) is identical to Eq. (18).

A.3. Equilibrium condition

At equilibrium, the chemical potential of adsorbed α must be equal to that of species α in free gas phase, so that $\mu_s = kT\ln\frac{\theta}{1-\theta} + \mu_s^{\sigma} \equiv \mu_g$, which is identical to the equilibrium condition expressed in Eq. (19), and thus yields the same expression for θ as given in Eqs. (20a) and (20b).

Appendix B. Kinetic methods

B.1. Rate of adsorption

Once again, for a total population of adsorption sites n_s (fixed), we assume that each adsorption site remains empty or else takes up one gas molecule, and that there is no interaction between adsorbed molecules. When n ($n < n_s$) molecules are adsorbed, the rate of adsorption by the remaining adsorption sites is

$$R_+ = f_+(n_s - n) \tag{34}$$

Here f_+ represents the frequency (probability) of one single diffusing gas molecule jumping over an energy barrier μ_e into the potential well associated with the adsorption site, yielding,

$$f_+ = \nu_+ \exp\left[\frac{-(\mu_e - \mu_g)}{kT}\right] \tag{35}$$

where ν_+ is the self-vibration rate of the diffusing gas molecule. The quantity μ_g represents the chemical potential of a single diffusing gas molecule (Fig. 2), which is equal to the potential in the free gas phase expressed as Eq. (7).

B.2. Rate of desorption

The rate of desorption of n molecules that are trapped in the adsorption sites is

$$R_- = f_- n \tag{36}$$

where f_- represents the frequency (probability) of one single gas molecule that jumps out of the adsorption site, written

$$f_- = \nu_- \exp\left[\frac{-(\mu_e - \mu_s^{\sigma})}{kT}\right] \tag{37}$$

Here ν_- is the self-vibration rate of the adsorbed molecule. μ_s^{σ} is the chemical potential of a single adsorbed molecule expressed by the Eq. (5b) (see Fig. 2).

B.3. Equilibrium condition

At equilibrium, the rate of adsorption must equal that of desorption, so that $R_+ = R_-$. Using Eqs. (7) and (34)-(37) gives

$$\frac{n}{n_s - n} = \frac{\nu_+}{\nu_-}\exp\left(\frac{\mu_{g0} - \mu_s^{\sigma}}{kT}\right)a_g \tag{38}$$

Assuming $\frac{\nu_+}{\nu_-} \approx 1$, inserting $\theta = \frac{n}{n_s}$, and rearranging, gives the expression for adsorbed concentration

$$\theta = \frac{a_g \exp\left(\frac{\mu_{g0} - \mu_s^{\sigma}}{kT}\right)}{1 + a_g \exp\left(\frac{\mu_{g0} - \mu_s^{\sigma}}{kT}\right)} \tag{39}$$

Using Eq. (5a), (5b) and (5c) for μ_s^{σ}, Eq. (39) becomes Eqs. (20a) and (20b).

References

Biot, M.A., 1941. General theory of three-dimensional consolidation. J. Appl. Phys. 12, 155–164.

Busch, A., 2005. Thermodynamic and Kinetic Processes associated with CO_2-Sequestration and CO_2-Enhanced Coalbed Methane Production from unminable Coal Seams. Bibliothek der RWTH Aachen.

Busch, A., Gensterblum, Y., 2011. CBM and CO_2-ECBM related sorption processes in coal: A review. Int. J. Coal Geol. 87, 49–71.

Bustin, R., Clarkson, C., 1998. Geological controls on coalbed methane reservoir capacity and gas content. Int. J. Coal Geol. 38, 3–26.

Butt, H.-J., Graf, K., Kappl, M., 2006. Physics and chemistry of interfaces. John Wiley & Sons.

Chang, R., 2000. Physical chemistry for the chemical and biological sciences. University Science Books.

Cui, X., Bustin, R.M., Chikatamarla, L., 2007. Adsorption-induced coal swelling and stress: Implications for methane production and acid gas sequestration into coal seams. J. Geophys. Res. Solid Earth 112.

Day, S., Sakurovs, R., Weir, S., 2008. Supercritical gas sorption on moist coals. Int. J. Coal Geol. 74, 203–214.

Day, S., Fry, R., Sakurovs, R., Weir, S., 2010. Swelling of coals by supercritical gases and its relationship to sorption. Energy Fuel 24, 2777–2783.

Day, S., Fry, R., Sakurovs, R., 2011. Swelling of moist coal in carbon dioxide and methane. Int. J. Coal Geol. 86, 197–203.

Dutta, P., Bhowmik, S., Das, S., 2011. Methane and carbon dioxide sorption on a set of coals from India. Int. J. Coal Geol. 85, 289–299.

Espinoza, D., Vandamme, M., Pereira, J.-M., Dangla, P., Vidal-Gilbert, S., 2014. Measurement and modeling of adsorptive–poromechanical properties of bituminous coal cores exposed to CO_2: Adsorption, swelling strains, swelling stresses and impact on fracture permeability. Int. J. Coal Geol. 134, 80–95.

Fitzgerald, J., Pan, Z., Sudibandriyo, M., Robinson Jr., R., Gasem, K., Reeves, S., 2005. Adsorption of methane, nitrogen, carbon dioxide and their mixtures on wet Tiffany coal. Fuel 84, 2351–2363.

Freudenberg, U., Lou, S., Schlüter, R., Schütz, K., Thomas, K., 1996. Main factors controlling coalbed methane distribution in the Ruhr District, Germany. Geol. Soc. Lond., Spec. Publ. 109, 67–88.

Gensterblum, Y., Merkel, A., Busch, A., Krooss, B.M., 2013. High-pressure CH_4 and CO_2 sorption isotherms as a function of coal maturity and the influence of moisture. Int. J. Coal Geol. 118, 45–57.

Gensterblum, Y., Busch, A., Krooss, B.M., 2014. Molecular concept and experimental evidence of competitive adsorption of H_2O, CO_2 and CH_4 on organic material. Fuel 115, 581–588.

Gray, I., 1987. Reservoir engineering in coal seams: Part 1-The physical process of gas storage and movement in coal seams. SPE Reserv. Eng. 2, 28–34.

Hill, T.L., 2012. An introduction to statistical thermodynamics. Courier Corporation.

Hol, S., Spiers, C.J., 2012. Competition between adsorption-induced swelling and elastic compression of coal at CO_2 pressures up to 100 MPa. J. Mech. Phys. Solids 60, 1862–1882.

Hol, S., Peach, C.J., Spiers, C.J., 2011. Applied stress reduces the CO_2 sorption capacity of coal. Int. J. Coal Geol. 85, 128–142.

Hol, S., Peach, C.J., Spiers, C.J., 2012a. Effect of 3-D stress state on adsorption of CO_2 by coal. Int. J. Coal Geol. 93, 1–15.

Hol, S., Spiers, C.J., Peach, C.J., 2012b. Microfracturing of coal due to interaction with CO_2 under unconfined conditions. Fuel 97, 569–584.

Langmuir, I., 1918. The adsorption of gases on plane surfaces of glass, mica and platinum. J. Am. Chem. Soc. 40, 1361–1403.

Laubach, S., Marrett, R., Olson, J., Scott, A., 1998. Characteristics and origins of coal cleat: A review. Int. J. Coal Geol. 35, 175–207.

Laxminarayana, C., Crosdale, P.J., 1999. Role of coal type and rank on methane sorption characteristics of Bowen Basin, Australia coals. Int. J. Coal Geol. 40, 309–325.

Levine, J.R., 1993. Coalification: The evolution of coal as source rock and reservoir rock for oil and gas: Chapter 3.

Levine, J.R., 1996. Model study of the influence of matrix shrinkage on absolute permeability of coal bed reservoirs. Geol. Soc. Lond., Spec. Publ. 109, 197–212.

Liu, J., Chen, Z., Elsworth, D., Qu, H., Chen, D., 2011. Interactions of multiple processes during CBM extraction: A critical review. Int. J. Coal Geol. 87, 175–189.

Liu, J., Peach, C.J., Zhou, H., Spiers, C.J., 2015. Thermodynamic models for swelling of unconfined coal due to adsorption of mixed gases. Fuel 157, 151–161.

Mares, T.E., Moore, T.A., Moore, C.R., 2009. Uncertainty of gas saturation estimates in a subbituminous coal seam. Int. J. Coal Geol. 77, 320–327.

Merkel, A., Gensterblum, Y., Krooss, B.M., Amann, A., 2015. Competitive sorption of CH_4, CO_2 and H_2O on natural coals of different rank. Int. J. Coal Geol. 150, 181–192.
Moore, T.A., 2012. Coalbed methane: A review. Int. J. Coal Geol. 101, 36–81.
Myers, A., 2002. Thermodynamics of adsorption in porous materials. AICHE J. 48, 145–160.
Myers, A., Monson, P., 2002. Adsorption in porous materials at high pressure: theory and experiment. Langmuir 18, 10261–10273.
Ottiger, S., Pini, R., Storti, G., Mazzotti, M., 2008. Competitive adsorption equilibria of CO_2 and CH_4 on a dry coal. Adsorption 14, 539–556.
Pan, Z., Connell, L.D., 2007. A theoretical model for gas adsorption-induced coal swelling. Int. J. Coal Geol. 69, 243–252.
Pan, Z., Connell, L.D., 2012. Modelling permeability for coal reservoirs: A review of analytical models and testing data. Int. J. Coal Geol. 92, 1–44.
Pini, R., Ottiger, S., Burlini, L., Storti, G., Mazzotti, M., 2010. Sorption of carbon dioxide, methane and nitrogen in dry coals at high pressure and moderate temperature. Int. J. Greenh. Gas Control 4, 90–101.
Pone, J.D.N., Halleck, P.M., Mathews, J.P., 2009. Sorption capacity and sorption kinetic measurements of CO_2 and CH_4 in confined and unconfined bituminous coal. Energy Fuel 23, 4688–4695.
Setzmann, U., Wagner, W., 1991. A new equation of state and tables of thermodynamic properties for methane covering the range from the melting line to 625 K at pressures up to 100 MPa. J. Phys. Chem. Ref. Data 20, 1061–1155.
Tuin, G., Stein, H., 1995. The excess Gibbs free energy of adsorption of sodium dodecylbenzenesulfonate on polystyrene particles. Langmuir 11, 1284–1290.
Wang, H., 2000. Theory of linear poroelasticity with applications to geomechanics and hydrogeology. Princeton University Press.
Weniger, P., Francú, J., Hemza, P., Krooss, B.M., 2012. Investigations on the methane and carbon dioxide sorption capacity of coals from the SW Upper Silesian Coal Basin, Czech Republic. Int. J. Coal Geol. 93, 23–39.
White, C.M., Smith, D.H., Jones, K.L., Goodman, A.L., Jikich, S.A., LaCount, R.B., DuBose, S.B., Ozdemir, E., Morsi, B.I., Schroeder, K.T., 2005. Sequestration of carbon dioxide in coal with enhanced coalbed methane recovery a review. Energy Fuel 19, 659–724.